Department of Precision and Microsystems Engineering

Design of a constant moment crease for use in neutrally stable origami

Edward van Wijk

Report no : 2021.048
Coach : Dr. ir. G. Radaelli
Professor : Prof. dr. ir. J.L. Herder
Specialisation : MSD
Type of report : Master Thesis
Date : 24 August 2021

Preface

Before you lies my thesis which is providing a first step towards neutrally stable origami. The main goal of this thesis was to complete the master Mechanical Engineering with the High Tech Engineering track. But besides this goal, it brought me a lot of knowledge. It was an interesting and challenging process for me which brought me joy and gave me a lot of learning experiences. In the field of Mechanical Engineering, origami is a very popular topic and I am sure other researchers will be interested in my graduation topic.

I would like to thank Giuseppe and Ali for their support. I could not have made this project a success without the weekly support of Giuseppe, which helped me to keep my code in MATLAB up and running. And the initial meetings with the two of you gave a clear direction to the project. Also, thanks to the other graduating students who provided me with great feedback during some productive and other less productive meetings.

Besides this I would like to thank my girlfriend Tamara, for all the mental support and good laughter. She kept me positive and motivated during the lockdown. Last but not least, I would like to thank Dobby and Tony, my cats who kept me company on my desk five days a week.

I hope you enjoy your reading,

Edward van Wijk
Delft, August 2021

Summary

The goal of this thesis is to look into the possibilities of making origami neutrally stable. This is wanted because the inherent stiffness of origami mechanisms introduces unwanted artifacts such as a higher actuation force, and the mechanism not following the theoretical kinematics. By making an origami mechanism neutrally stable the inherent stiffness of the pattern can be removed, and with that the unwanted artifacts as well.

Two different strategies are explored, both a form of static balancing. With static balancing, two elements are balanced against each other. In the origami application, this means that two creases are balanced against each other. For the first strategy, a negative stiffness crease is combined with a positive stiffness crease. And for the second strategy two equal but opposite constant moment creases are balanced. To achieve this a negative stiffness, or constant moment crease needs to be designed.

For the negative stiffness crease, a design was made where a flat sheet with a slot in the middle was prestressed into a saddle form. This showed bi-stable behavior, and with that negative stiffness. The range of negative stiffness was too short to be relevant for origami. And the prestressing proved hard to model. For the constant moment crease, a convex crease was designed, which did not need to be prestressed. This was easier to model, and three different geometries were found that showed a constant moment. By optimizing these geometries a constant moment over a range of 80° was found.

To check if the model is correct, a prototype experiment was performed. The optimized geometry was 3D printed and tested under the same boundary conditions that were present in the model. The results of the prototype experiment matched the results of the model, thereby validating it.

Contents

1

Introduction

Origami is usually known as an art form, where 3D-figures are created by folding flat sheets of paper. This has become a source of inspiration for designing mechanisms, because origami is scalable, and has the potential to switch between different states. This makes origami mechanisms applicable to many fields [1]. For these reasons origami mechanisms is a growing research field. This can be seen by looking at the papers containing ”Origami mechanisms” in google scholar, 75 % of these were written in the past four years.

Within most mechanisms there is usually an input and an output, where a force or displacement on the input actuates the output. In an origami pattern each cell acts like a separate mechanism with an input and an output, these are chained together so that the output of the one cell is also the input of the next cell. How the pattern deforms is often determined using the rigid origami concept. This breaks down the movement of the pattern to just its kinematics [2]. This is because the stiffness ratio between the facets and the creases is assumed to be infinite, so all the deformations in the pattern happen in the creases.

In reality however this is not what happens. The facets are not rigid but they have a stiffness, and so do the creases. This means that there is a finite stiffness ratio between the facets and the creases, and not all deformations happen in the creases anymore. This introduces artifacts in the system which will make it no longer follow the theoretical kinematics [3]. This can be seen in a simple origami tessellation. If one cell is completely folded all the other cells should also fold completely. But what happens is that the adjacent cells will only partly fold and cells even further away will hardly be affected by the first cell. This can be a problem in origami mechanisms. For example, when used as a transmission, the output will not necessarily follow the input in the intended way. Another advantage of mechanisms with theoretically correct kinematics is that they can be easily used for deployable structures. This is a structure that is folded such that it can be deployed in one continuous motion [4]. When the kinematics of such a structure are theoretically correct it can be fully deployed by only actuating one cell. So far researchers have focused on reducing the stiffness of the creases to approach the infinite stiffness ratio. This can be done by making the crease thinner, perforating the crease, or reducing the Young’s modulus of the crease. These methods are the focus of the literature survey which can be found in chapter 2. In this survey a research gap is found under prestress, what is meant with this is that the stiffness of origami mechanism can be removed with the use of prestress. This can be achieved with the technique of static balancing.

In static balancing two different elements are combined to create zero-stiffness. There are two ways to achieve this. Firstly, it is possible to create one element with a negative stiffness and combine this with an element that has an equally large positive stiffness [5]. This gives a downward sloped and an equally upward sloped moment-angle characteristic, these two elements need to be prestressed into the right position such that the two slopes added up equal zero, this will result in a combined moment-angle characteristic with a flat region at zero. Secondly, two constant moment elements can be combined. One of these elements needs to be flipped around, this will give the two elements an equal but opposite

constant moment. These will again need to be prestressed such that the constant moment ranges of the two elements overlap. Then together they will form a mechanism that is statically balanced. This was demonstrated by Radaelli, [6].

These two different methods can be applied to origami by using the creases as balancing elements. So either a crease with a negative stiffness is combined with a positive stiffness crease, or two constant moment creases are combined. A normal crease already has a positive stiffness, so to achieve this way of static balancing, either a negative stiffness crease, or a constant moment crease is needed.

In this thesis, multiple designs for both zero stiffness or constant moment creases are explored. With the goal to use them for statically balancing a Miura-ori pattern. This is achieved through modeling these creases in a FEM program and optimizing them for their needed properties, either negative stiffness or a constant moment, in their moment-angle characteristics.

In chapter 2, the literature survey which led to the idea of the thesis can be found. Then in chapter 3, the design of a constant moment crease, and its application into origami mechanisms is presented in a paper format. This is followed by the discussion and conclusion. In the appendixes some extra analyses are shown, as well as supplementary information, such as how the creases can be implemented into origami, the concept generation of both negative stiffness and constant moment creases, and details on how the modeling was performed.

2

Literature survey: Literature review on achieving theoretical kinematics in origami and metamaterial mechanisms

Literature review on achieving theoretical kinematics in origami and metamaterial mechanisms

Edward van Wijk

***Abstract*—Origami mechanisms are mechanisms that are created by folding a flat sheet into a 3D structure. These mechanisms are usually designed with the rigid origami method. Here it is assumed that the facets are infinitely stiff, and the creases are frictionless hinges. In reality, however, both the facets and the creases have a stiffness. This causes origami mechanisms to not follow their theoretical kinematics. In this review, an overview is given of the different methods that are used to approximate the theoretical kinematics in these mechanisms. These methods are categorized into four different techniques and these are subdivided into multiple strategies. Finally, a division is made between compliant and metamaterial mechanisms, and origami mechanisms. From the results, it can be concluded that decreasing the crease stiffness does not work well enough to create proper kinematics as it often has to be combined with a method from a different category. However, a research gap is found under prestress that offers the opportunity to decrease the crease stiffness to such a point that an origami mechanism can follow its theoretical kinematics.**

I. Introduction

Origami is the art of paper folding. In origami, flat paper sheets can be constructed into 3D structures. This is an attractive property for engineers as it allows the manufacturing of complex 3D shapes with simple 2D fabrication methods. Therefore there has been an increasing amount of research into using this concept to develop mechanisms. This can be seen from the dates of papers containing "origami mechanism" found in Google Scholar. Of these papers, 58% were written in the past four years.

What is often seen in mechanisms is that a force or displacement on one part moves another part of that mechanism. For an origami mechanism, this means that by actuating one cell of the pattern the whole pattern will move along. How this pattern will move is often determined using the rigid origami concept. Here the origami is modeled as rigid facets connected by frictionless hinges. This makes designing these mechanisms a matter of kinematics [25]. This is the case because the stiffness ratio between the facets and the creases is infinite. This means that all deformations happen in the creases and not in the facets. In reality, however, these origami facets are not rigid but have a certain stiffness, and the creases are not frictionless hinges but also have a stiffness. This results in a finite stiffness ratio which means that the facets will deform as well. Furthermore, the creases can also deform in other directions other than the bending direction because they are not ideal hinges. This introduces artifacts in the system which will make it no longer follow the theoretical kinematics [19]. This can be seen when a tessellation is locally actuated, in theory, all cells should have the same angles so the tessellation should deform globally, but in practice, the tessellation will only deform locally with the cells adjacent to the actuated cell compressing more than the cells further away.

In this literature review, the techniques that help origami mechanisms to follow their theoretical kinematics are explained and categorized. In this categorization, compliant mechanisms and metamaterial mechanisms are also included. This is done because some of the techniques that are seen in these areas could also be used in origami mechanisms. Thus including these other areas will give a better view of research gaps in origami mechanisms.

In the methods section, the proposed categories of the categorization will be explained. The strategies to achieve some of these categories will be explained in their 1 respective sections under the results. There, the found literature will also be categorized according to this categorization. For every strategy, compliant and metamaterial mechanisms will be discussed first, followed by origami mechanisms. In the discussion, the observed similarities between papers, which became apparent through the categorization, are discussed.

II. Methods

Most papers do not report on problems with the kinematical correctness of their mechanisms and use different methods to still allow their mechanisms to function properly. The techniques used were found in papers regarding origami, metamaterial, and compliant mechanisms. These techniques are divided into four categories (Fig. 1). The first category is *decreasing crease stiffness*. This is based on the fact that an infinite stiffness ratio between the facets and the creases is needed for proper kinematics. By decreasing the stiffness of the creases this can be approximated. The second category is *individual cell actuation*. Here every cell within the mechanism has its own actuator. When this actuation is equal over all cells, they will all move into the same shape. The third category is *external constraints*. This encompasses mechanisms that have external constraints or boundary conditions that only allow for movement following the theoretical kinematics. This is often accomplished by connecting multiple cells rigidly together and actuating them all at the same time. The final category is *real hinges*. This again uses the fact that an infinite stiffness ratio is needed. Hinges that are not compliant do not have a stiffness. Therefore, using these hinges as creases gives zero-stiffness creases. This results in an infinite stiffness ratio. To achieve the first two categories multiple strategies can be thought of. These will be discussed in their respective sections. Finally, for the first three categories and their strategies a division can be made between origami mechanisms and metamaterial or compliant mechanisms.

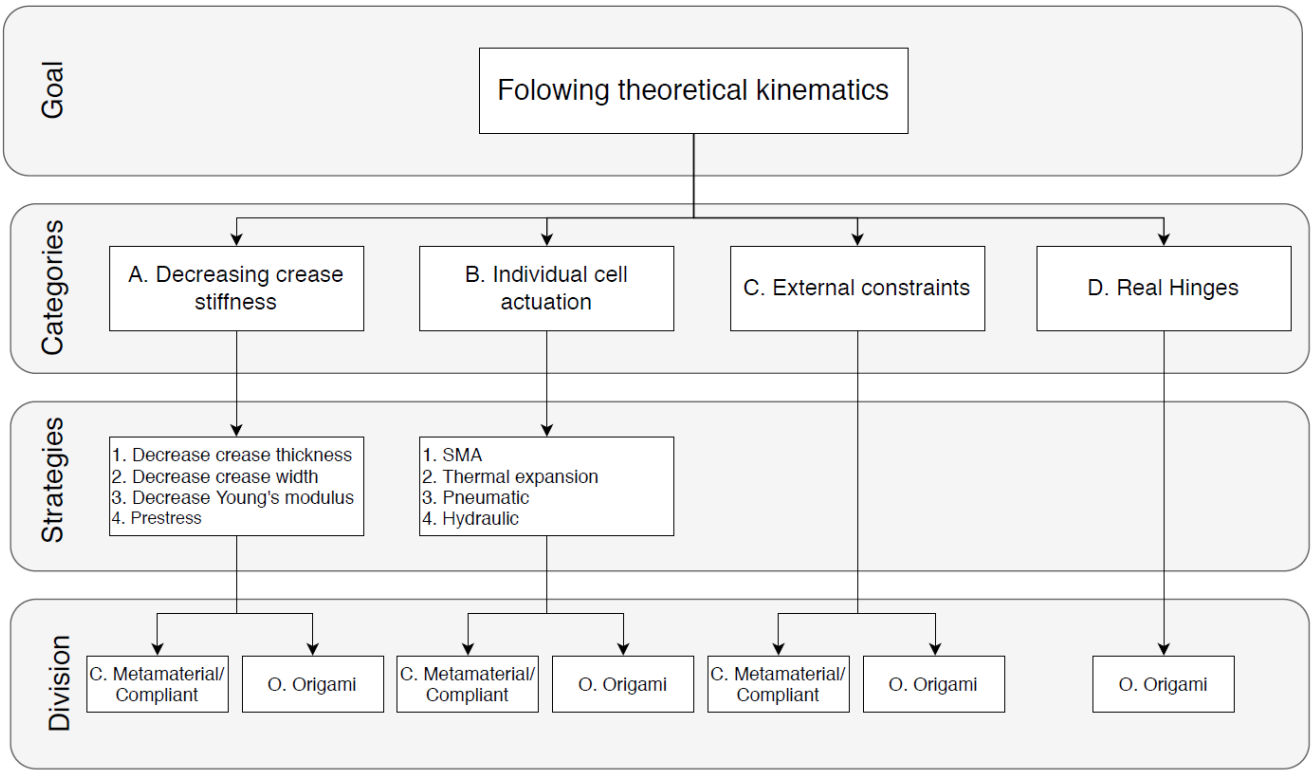

Fig. 1. Visualization of the proposed categorization.

The division between these two is that origami mechanisms can be folded flat, where metamaterial and compliant mechanisms are fabricated in 3D and will stay that way. For the fourth category, *real hinges*, this division is not made as using real hinges in a mechanism excludes it from being a compliant mechanism.

III. Results

A. Decreasing crease stiffness

In the rigid origami theory, it is assumed that the stiffness ratio between the facets and the creases is infinite. Because infinitely stiff facets do not exist, the only way to realize this is to reduce the crease stiffness to zero. If the creases have no stiffness at all, the mechanism will follow the theoretical kinematics. In origami, the important crease stiffness is its bending stiffness, for a flat crease with a rectangular cross-section this stiffness is defined by the expression: $K = \frac{EI}{L}$. Here E is the young's modulus. I is the area moment of inertia expressed in the thickness t and width w as $I = \frac{wt^3}{12}$. Finally, L is the length of the crease (Fig. 2). From this, there are four options to decrease the bending stiffness of a crease which are:

1) Decreasing the crease thickness
2) Decreasing the crease width
3) Decreasing the Young's modulus
4) Increasing the crease length

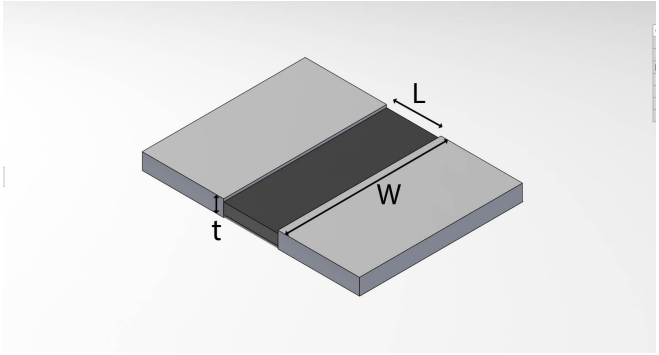

Fig. 2. Dimensions of the crease.

The most effective way to do this is by decreasing the thickness as this scales the stiffness by the power three [22]. Decreasing the width and Young's modulus is also often seen, but increasing the length is not. Although it does help to decrease the stiffness it also allows more motions like torsion which is not wanted in the creases. Therefore this technique is not used. Another method of decreasing the stiffness is using a prestressed counter stiffness. By prestressing, for example, a beam, into a buckled state, it can get a negative stiffness. By coupling this prestressed beam to a different element the stiffnesses can cancel each other, given that their stiffnesses are opposite but equal. This combination will result in a statically

balanced mechanism.

1) Decreasing crease thickness: **C.** Reducing material thickness to create a joint is common practice in compliant mechanism design. A notch joint is a clear example of this. In Howell's book, *compliant mechanisms* [8], a notch joint can be seen in multiple mechanisms. For example a bistable switch (Fig. 3). Another example is the microgripper from Raghavendra [24] (Fig. 4). Here the arm pivots around the right hinge while it is being actuated by the piston on the left. The metamaterial mechanisms from Ion [10] can also be

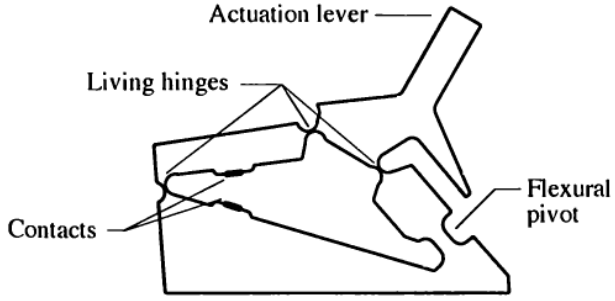

Fig. 3. Bistable switch with notch joints, Howell [8].

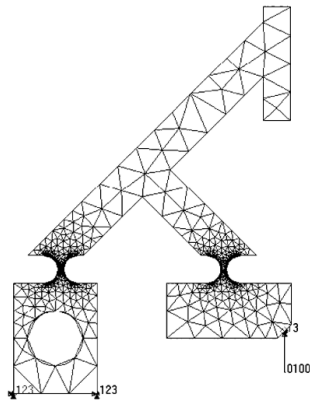

Fig. 4. Mesh of one arm of a microgripper, Raghavendra [24].

classified under decreasing crease thickness. The mechanisms are constructed by square cells that can shear, these cells are laser cut from rubber, or 3D printed. In the cut pattern, the corners of the cell are left thinner than the edges (Fig. 5). The produced mechanisms are in the centimeter range, but with the laser cutting technique, the sizes could be increased or decreased. How small they can be produced is dependent on the resolution of the laser cutter. On the other end, the maximum size depends on the bed size. Due to the overall flexibility of the mechanisms they do not follow the proper kinematics too well.

O. In Kuribayashi [15], a self-deployable origami stent-graft is described. This stent can be folded compactly to be inserted more easily into an artery, and will then deploy automatically.

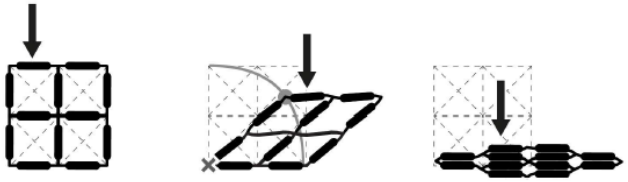

Fig. 5. Shear cells where the corners are thinner than the edges, Ion [10].

The stent is made out of an SMA foil, in this foil grooves are etched which define the crease pattern (Fig. 6). Due to the etching technique that is used this is only possible for thin materials, and thus, for small mechanisms. The foil used for the stent is 0.070 mm thick, and the stent is approximately 5 cm long. Reducing the crease thickness was not enough to get proper kinematics, this can be concluded from the fact that all the creases still need to be individually actuated. Onal [22]

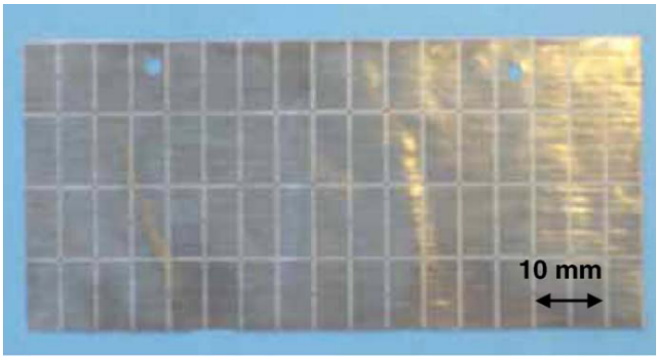

Fig. 6. SMA foil with etched creases, Kuriabayashi [15].

tried to use thinner creases in his worm robot. This robot is designed using a waterbomb base pattern which is rolled into a tube (Fig. 8). This pattern, which has a negative poison ratio, can contract axially which gives it a peristaltic motion. This, combined with frictional anisotropy, i.e. the frictional forces in the backward direction are greater than those in the forward direction, yields a net forward motion. The robot is fabricated from a polymer sheet. The creases were engraved at first. This, however, did not work properly. The engraving was only done on one side of the sheet, which caused an asymmetry in the folding, also repeatability was hard to achieve as the crease lines were weakened by the laser. Another example where thin creases were not adequate is from Iniguez-Rabago [9]. In his paper research is done into the multistability of an origami-inspired metamaterial. The metamaterial is constructed by extruding different kinds of polyhedrons. Theoretically, these structures should have multiple stable configurations. First, $50\mu m$ thick mylar is used for the hinges. However, with these hinges, the theoretical stable states were non-existent in the produced prototypes.

2) Decreasing crease width: **C.** In Sung [27], research is done into foldable joints. These joints are designed using the origami principle. The fold lines of the origami pattern are

perforated during the laser cutting process, which effectively decreases the width of the crease. The joints are made from 0.051 mm and 0.127 mm thick polyester film. This method can be applied on the centimeter scale, for thicker hinges it probably would not work that well, as crease stiffness scales to the power three with the thickness. How well the theoretical kinematics are followed is not shown in the paper, but looking at the figures does give insight into this (Fig. 7). The facets are still very thin and far from rigid, this gives the impression that movements not allowed by the theoretical model are still possible.

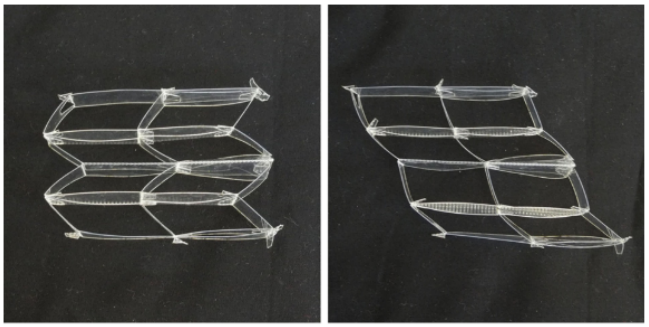

Fig. 7. Foldable joints with perforated creases, Sung [27].

O. The perforation technique is also used for a worm robot by Onal [22], which has been discussed previously. To remedy the asymmetry of the engraved crease, it is now perforated (Fig. 8). The stiffness is still decreased but the crease is now symmetric and not the whole length of the crease is affected by the laser making the process more repeatable. Finally, the required stiffness of the creases is easily controlled by adjusting perforation density. Just like the foldable joints, the worm robot is in the centimeter scale, but as explained above it is difficult to scale up. The theoretical kinematics are still not fully realized as the robot needs an actuator throughout all the individual cells.

3) Decreasing Young's modulus: **C.** In compliant mechanisms, joints can also be made of flexible materials. Some theory on these joints is explained by Bejgerowski [4] (Fig. 9) and Gouker [7] (Fig. 10). A downside of using two materials is that manufacturing becomes more complicated. In these papers, multi-material molding is used to manufacture these joints which makes the process easier.

O. Kaspersen [13] made a design for a flat kirigami actuator that lifts a part out of its plane when it is pulled on (Fig. 11). The actuator is made from a combination of wood and fabric. The wood is used for the stiff facets, these facets are put on a fabric pattern which is cut in the shape of the actuator. The size of the actuator is in the centimeter scale, with the used fabrication technique it is likely that this could be scaled up to meters, like suggested in the paper. The theoretical kinematics seem to be followed reasonably, this is in part due to the large stiffness ratio between the wooden facets and fabric hinges, but also because only one cell is made leaving it no room but to follow the proper kinematics. In Tachi [28] a combination of

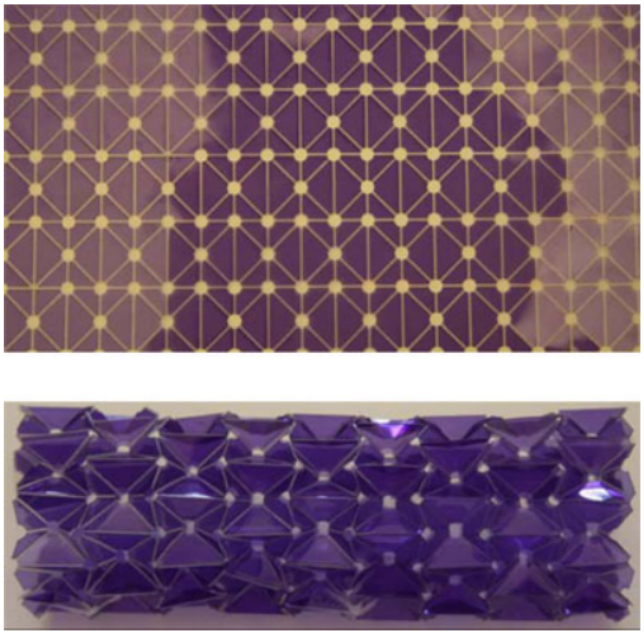

Fig. 8. Worm robot with perforated creases, Onal [22].

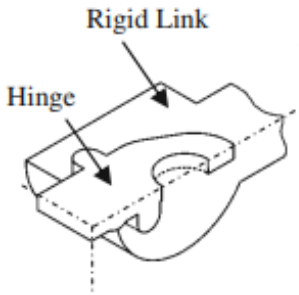

Fig. 9. A rigid link is connected to a flexible hinge, Bejgerowski [4].

rigid panels on fabric is used as well(Fig. 12). The prototype that is manufactured is of the decimeter scale, but the paper also envisions using this principle at the meter scale or even bigger. No prototypes were constructed that show how well the theoretical kinematics are followed, but as the panels are much stiffer than the fabric it would probably perform well. Iniguez-Rabago [9] also uses a two material approach for an origami mechanism. As discussed before, at first a thin mylar was used for the hinges, but as this did not work the mylar was replaced by elastomeric hinges with a lower Young's modulus. This increased the number of theoretical stable points that were found from 0 to 6 out of 8 (Fig. 13). This is not completely proper, but it is a good result. The prototypes are made at the centimeter scale, scaling this up or down should not be a problem as the stiffness ratio between the facets and the creases will stay the same. However, its possible size will be limited by the resolution of the 3D-printer and its maximum size. An origami soft gripper developed by Li [16], comprises of two different materials. Rigid PET facets are glued on two

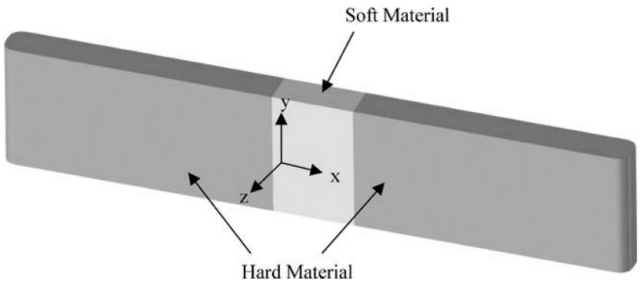

Fig. 10. Soft material is used in between hard material to create a hinge, Gouker [7].

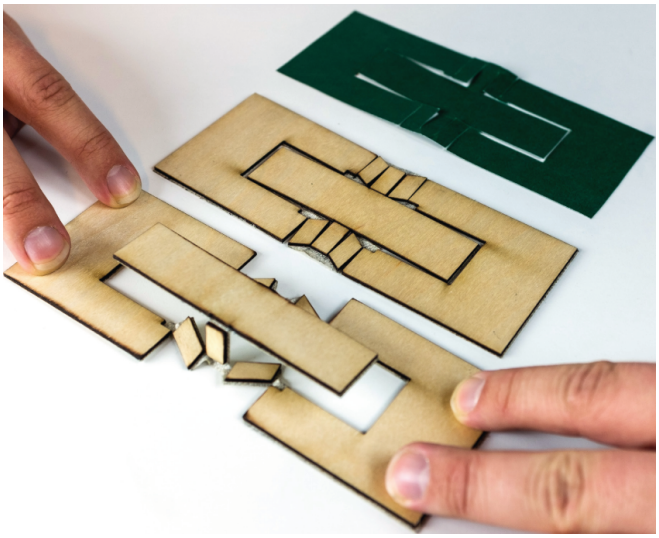

Fig. 11. Flat kirigami actuators with rigid wooden facets on a fabric, Kaspersen [13].

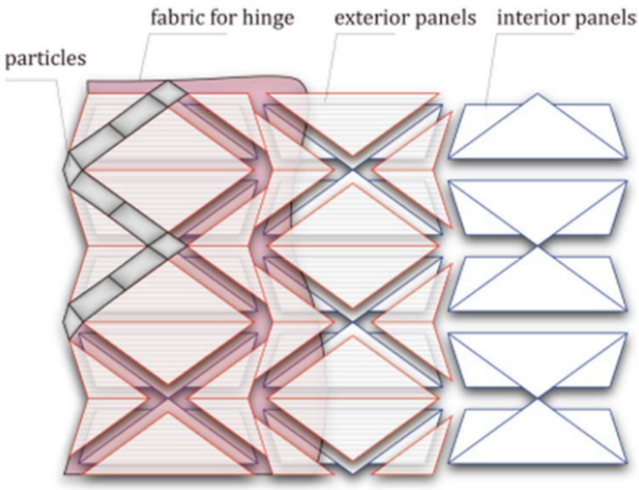

Fig. 12. Rigid panels on a fabric, Tachi [28].

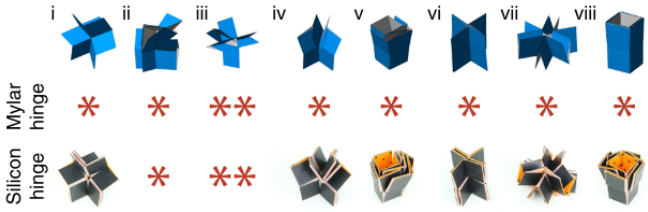

Fig. 13. Multistable states of a prismatic metamaterial. No stable states are found with the mylar hinges, and six are found with the silicon hinges, Iniguez-Rabago [9].

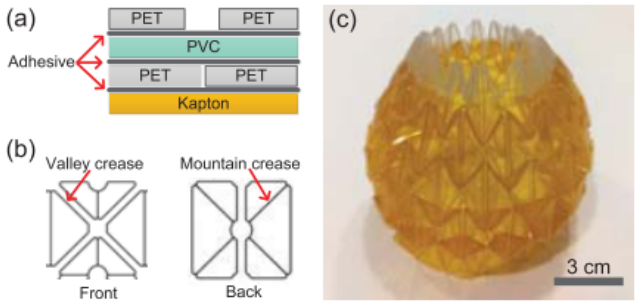

Fig. 14. Origami gripper (a) Two layers of PET are glued onto a PVC layer. (b) For valley creases, a gap is left between the PET facets and for mountain creases, a cut is made. (c) Prototype of the gripper, Li [16].

sides of a flexible PVC layer. For valley folds a gap is left between the PET, for mountain folds a cut is made (Fig. 14). The size of the gripper is in the centimeter scale and could be scaled up as the stiffness ratio between the PET facets and PVC creases do not scale with size. The gripper does not follow the theoretical kinematics too well, but as it is a soft gripper this does actually help. This way the gripper can deform around asymmetric objects to grip them from all sides. It is also helped by vacuum actuation which deforms the whole gripper at the same time.

4) Prestress: **C.** In Merriam [20], prestress is used to reduce the stiffness of a compliant joint. This concept could also be applied to origami mechanisms and has the potential to completely remove the stiffness of the creases resulting in a perfect following of the theoretical kinematics. However, there are no publications that look into this possibility.

B. Individual cell actuation

The kinematics of an origami mechanism can be improved by actuating all its cells or creases individually. When each cell is locally subjected to the same actuation force, the whole mechanisms will have a uniform global deformation. This is also what should happen according to the theory. Actuating all cells individually seems like a tedious task, especially when there are multiple cells. However, with the methods found in the literature, this can be easily done. Different strategies were found to conveniently actuate multiple cells. The first one that will be looked at is shape memory alloy (SMA). This is an alloy that can be deformed when it is cold, but it will return to its undeformed shape when heated up. This property can be used in origami mechanisms to actuate all the cells at once by heating the whole mechanism. Another method that uses temperature is based on thermal expansion. Materials will expand when they are heated up and shrink when cooled. This can be used as a simple linear actuator, but by connecting two materials with different thermal expansion coefficients it can also generate a bending motion. This is due to the fact that one layer will expand more than the other layer it is connected to, this will generate a bending of both materials. The third strategy is using pneumatics. By pushing pressurized air into a closed space this can be inflated to actuate a mechanism, then by depressurizing, the mechanism can return to its original state. This same method can also be used using fluids, making hydraulics the final strategy under the category *individual cell actuation*.

1) SMA: **C.** SMA is used as an actuator in compliant mechanisms. In Sreekumar [26], a platform mounted on an elastic pillar is connected to three SMA wires which can be used to move the platform (Fig. 15). It is also used in Balaji [3]. Here a pipe crawler is designed which is a mechanism that can crawl along a pipe. Two rings are connected by an SMA actuator, one ring clamps the pipe while the other one is released and pulled towards the clamped ring. They then switch state and the loose ring is pushed away, this gives a forward motion which is caused by the SMA actuator.

O. SMA is also used by Kim [14] to create a self-deployable origami structure. The SMA is woven through the whole structure (Fig. 17), and when it is heated up the origami deforms such that the shape is locked. This greatly increases the total stiffness of this mechanism. An origami sheet of 89 by 63 mm is used, with that, the structure belongs in the centimeter scale. The actuation of the structure does not generate a movement but only increases its stiffness by locking the cell. This locking is achieved by heating the whole structure to 70 °C. Because the structure has to cool down naturally, the actuation frequency has to stay low. However, this is also what the structure is designed for. The prototype in the fully activated state is 4 cm tall. Scaling up the structure and the thickness of the SMA wire would contribute to an even longer cooldown time. Using the SMA actuators on every cell makes sure that the theoretical kinematics are followed. SMA is also used in the worm robot of Onal [22], which also features perforated creases to reduce its stiffness. A single SMA wire is woven through each segment of the origami tube (Fig. 18), this makes the contractions around the perimeter of the tube more even. The SMA wire takes 6 seconds to passively cool down before it can be contracted again. This has a big influence on the actuation frequency and makes the robot slow at an average forward velocity of 18.5 mm/min. As mentioned before the robot is in the centimeter scale, scaling up the robot and with that, the SMA wires would increase the cooldown time, thus this is not feasible. Reducing its size would however have a positive effect on the cooldown time. Because one wire is used and the contraction over the whole tube is even the robot follows the theoretical kinematics. The stent-graft from Kuribayashi [15], which is also discussed under decrease crease thickness (Fig. 6), also uses SMA. Opposed to the designs of Kim and Onal, here the entire mechanism is made from an SMA foil. At a temperature of 46 °C, the stent will deploy on its own. It takes approximately 60 seconds to fully deploy. For most mechanisms this is too slow,

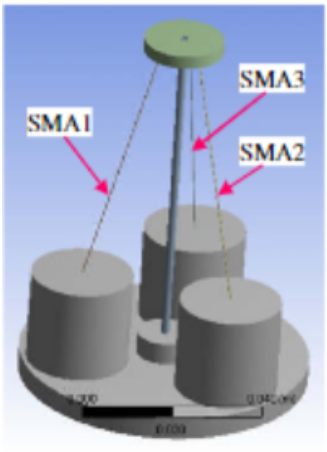

Fig. 15. A platform on an elastic pole connected to three SMA wires, Sreekumar [26].

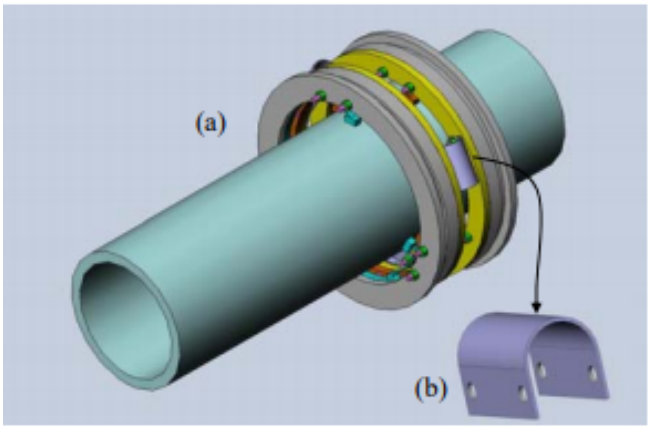

Fig. 16. (a) The pipe crawler with (b) an SMA U-shape that actuates it, Balaji [3].

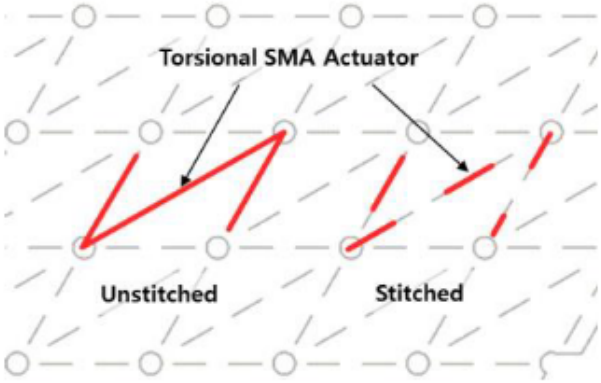

Fig. 17. SMA wires are woven through an origami pattern to act as its actuator, Kim [14].

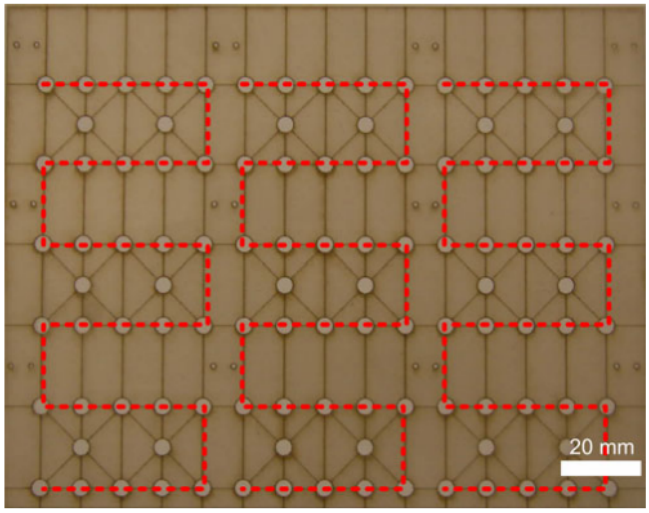

Fig. 18. SMA wire (red dashed line) woven through the origami pattern of a robot worm, Onal [22].

however as a stent only needs to deploy once and then never again, speed is not a problem for this application. The SMA foil has a thickness of 0.070 mm, and the length of the stent is approximately 5 cm. The thicker the foil the longer it will take to fully deploy the stent. Because the whole stent heats up as one, all the cells of the pattern will deform equally. This means that the stent follows its theoretical kinematics.

2) Thermal expansion: **C.** Thermal actuation is mostly seen in micromechanisms. This is because on a small scale it is easier to change material temperature, which is the driving force of a thermal actuator. Baker [2] designed a switch that uses thermal actuators in a fishbone pattern. When the temperature is increased all the skewed beams will expand and move the middle beam they are connected to. Other examples can be seen in Howell [8].

O. Just like with SMA for this method the system is actuated by temperature change, however, Boatti [5] uses a bilayer plate with two different materials that have a different thermal expansion coefficient. When heated up one layer will expand more than the other and the plate will bend. This is applied on a Miura-ori pattern where half of one cell consists out of the bilayer plate, and the other half is just a monolayer plate (Fig. 19). When the temperature changes, the crease angle of the bilayer plate will change. Heating the Miura-ori sheet from 20 °C to 70 °C expands the sheet as expected. Because every cell deforms the same amount the expansion is uniform over the whole sheet as the theoretical kinematics would predict. As it is actuated by temperature and it takes time to heat up and cool down the origami this actuation technique is quite slow. The size of the origami is in the decimeter range, it could be scaled down, but scaling it up more would mean that the actuation frequency would drop even more. This is because the thicker the sheet, the more time heating, and cooling it takes.

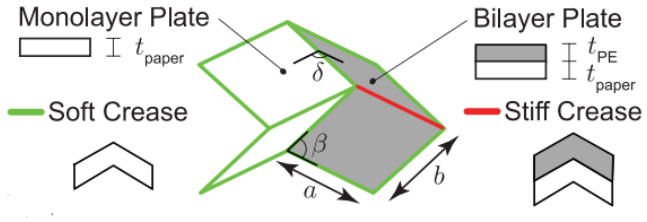

Fig. 19. A Miura-ori cell with on one side a monolayer plate, and on the other side a bilayer plate, Boatti [5].

3) Pneumatic: **C.** Pressurized air is used by Overvelde [23] to make a mechanical metamaterial. In their approach, an origami-like design is used where each cell is an extruded cube (Fig. 20a). A combination of multiple of these cells forms a mechanism which can transform into multiple shapes. To switch between these shapes every extrusion of the cube has an air pocket on its hinge which can be pressurized to actuate that hinge (Fig. 20b). By actuating the hinges in the correct order the whole structure can move into different states. The prototype is made from three layers, two outer layers of polyethylene terephthalate and one inner layer of double-sided tape. The cells are folded from these layers and using revealed parts of the tape to connect them. The whole structure is on the decimeter scale. It can be actuated at a high frequency as, unlike with the previous two strategies, actuation is active in both ways. This means that both the pressurization and depressurization can be done with an actuator instead of having to wait for one of these steps. Because not every hinge in the mechanism has an air pocket the theoretical kinematics are not followed exactly, however for this application enough actuators are implemented to make it work.

O. A different way to utilize air pressure is to cover an origami skeleton with an airtight layer, by adding negative pressure to this airtight mechanism the origami skeleton is pressed on from all sides. In Deshpande [6], the origami skeleton is a bellow pattern that can expand and contract. Adding a negative pressure will contract the skeleton allowing

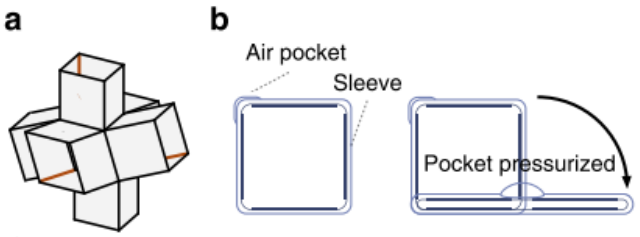

Fig. 20. (a) A unit cell made of an extruded cube. (b) Extrusion with air pocket on one hinge which can be pressurized to fold the cell, Overvelde [23].

it to be used as an actuator. The skeleton is made from paper and is covered with latex. The actuator is 20 cm long in its most stretched position. The actuator can be actuated fast as the pressure can be increased and decreased immediately after each other. The proper kinematics are also followed well due to the latex pressing on the whole skeleton at the same time. The origami soft gripper from Li [16] (Fig. 14) also uses pneumatic actuation. The structural origami is encased by an airtight latex-rubber balloon. The whole gripper is only a few centimeters long but can hold loads up to 120 N. This indicates that scaling up the mechanism would not be a problem for the power that the vacuum pump can deliver. Nothing is reported on how fast the gripper is actuated but with the pneumatic actuation, it will be relatively quick. With the overall actuation of the gripper, the theoretical kinematics are followed better, however, as mentioned earlier it is a soft gripper that deforms to the shape of the gripped object. This means that it is not always wanted to follow the theoretical kinematics properly.

4) Hydraulic: **O.** Li [18] investigated the possibilities for pneumatics in origami. Two Miura-ori sheets are put on top of each other with space in between which acts as a fluid channel. By regulating the volume of the fluid in these channels the size of the structure can be increased or decreased. The prototype is manufactured at the centimeter scale, this could be scaled up as hydraulics offer the possibility for high pressure which can also move larger actuators. The actuation speed is also fast as like with air pressure, an immediate switch can be made between inflation and deflation. Using pressure in between two sheets assures an even distribution of the force per cell. This results in a good following of the theoretical kinematics. In

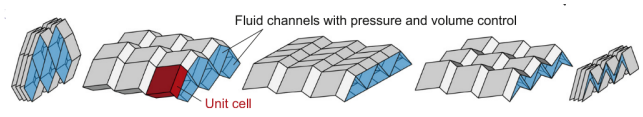

Fig. 21. Two Miura-ori sheets on top of each other with fluid channels in between them, Li [18].

another paper [17] Li looks at a slightly different approach. Here an origami structure is used as a skeleton, around which a fluid-tight layer is put. By filling this layer with fluid, or extracting it, the skeleton is extended or shortened. The actuators are manufactured at both the centimeter and the decimeter scale. The second one can lift a 22 kg load 20 cm. This load indicates that bigger actuators would be possible as well. Again hydraulics offer the opportunity to actuate the mechanism fast. Due to the distributed pressure, the skeleton deforms as the theoretical kinematics would predict.

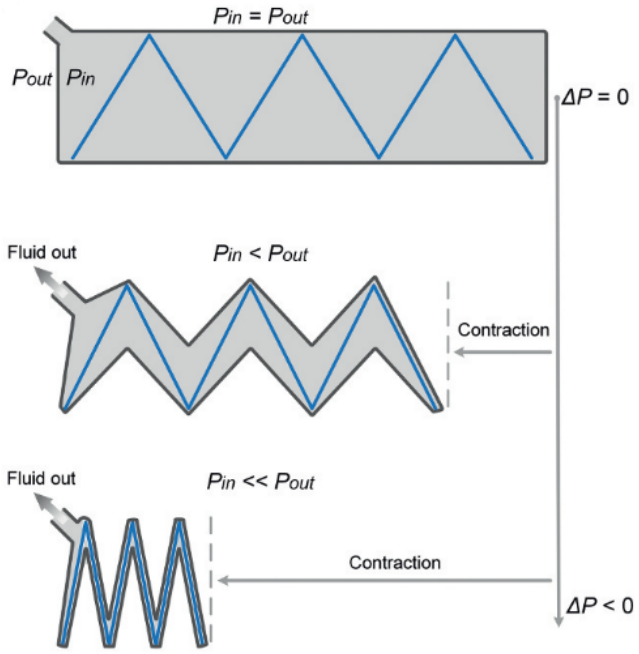

Fig. 22. An origami skeleton with a fluid-tight layer around it, enabling the contraction of the skeleton, Li [17].

C. External constraints

External constraints can be used to force origami and metamaterial mechanisms into their designed kinematics. By placing constraints in the right positions motions of these mechanisms that are not part of the theoretical kinematics can be stopped. **C.** In a paper by Ion [11] a design for changing material textures is proposed. This mechanism is originally smooth, but when it is compressed spikes will pop out (Fig. 23). This mechanism is implemented for different uses. One of the prototypes is a shoe that can change the grip of its sole (Fig. 25). In this case, the designed mechanism is the shoe sole. One end of the sole is fixed to the back of the shoe while the other end is connected to a string. Its state is manually changed by pulling this string which compresses the sole. This leaves no room for the mechanism to move differently than the theoretical kinematics. Another application is a door handle whose texture can be changed. A knob at the end of the handle can be turned, this winds up strings that are connected to the other end of the handle. The handle is now compressed between the knob and its end (Fig. 24). This again makes sure the mechanism follows its theoretical kinematics. The mechanism is manufactured using a 3D printer.

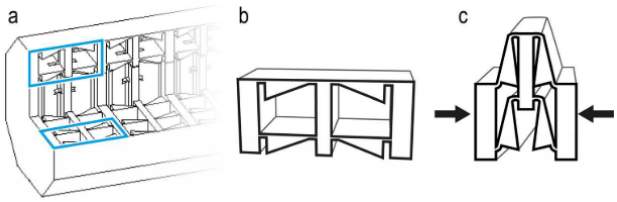

Fig. 23. (a) Textured objects consist of many (b) unit cells, which (c) pop out of the object's surface when compressed, Ion [11].

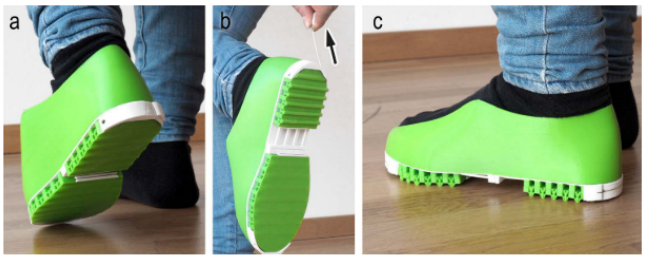

Fig. 24. (a) This shoe sole is flat by default. (b) The user transforms it into a treaded sole it by pulling a string, e.g., when it starts snowing. (c) Note that the sole is functional and robust enough to walk on, Ion [11].

External constraints are also used by Lin [19] at the micro-scale. Here a metamaterial is designed using Miura-ori tubes which are coupled together to form one mechanism. This is produced using a two-photon polymerization direct laser writing technique. The whole structure is around $100\mu m$, with this technique this cannot be scaled up as it is only possible to print small objects with it. The goal of the mechanism is to have different stiffness in different directions. This is tested by putting the mechanism in between two plates that compress it. By having the plates as boundary conditions the mechanism will compress as the theoretical kinematics predict. The metamaterial mechanisms from Ion [10], which are also discussed under Decreasing crease thickness, also use external boundaries. The shear cells that are used are encased by rigid beams on all sides which only leave one degree of freedom for the whole cell. This has as a result that the mechanisms follow the theoretical kinematics.

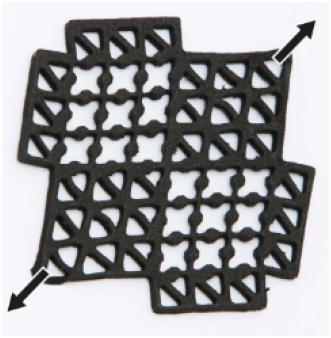

Fig. 27. Shear cells that are constrained at the outside, Ion [10].

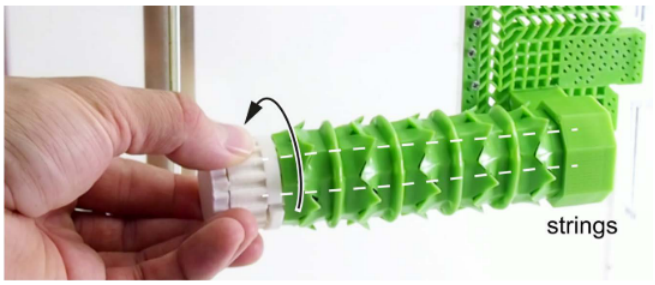

Fig. 25. A door handle whose texture can be changed by turning the knob on the front, Ion [11].

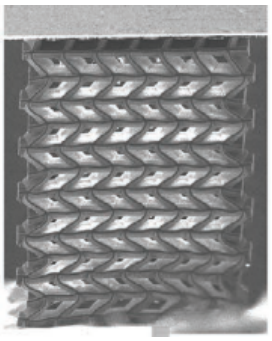

Fig. 26. Metamaterial made of Miura-ori tubes which is clamped between two plates, Lin [19].

O. Babaee [1], uses these constraints for a kirigami shoe grip. This is a flat mechanism that can be fixed underneath a shoe and when actuated becomes spiky to increase the grip of the shoe. The kirigami sheet is rigidly connected to the front and back of the sole, the actuation happens when the curvature of the sole changes and with that the kirigami is extended (Fig. 28). Because the sheet is connected over the full length across the front and back, all the cells in between these connection points are actuated with the same force and follow the theoretical kinematics. The grips are laser cut from 0.051 mm thick steel and are 11 x 7 cm.

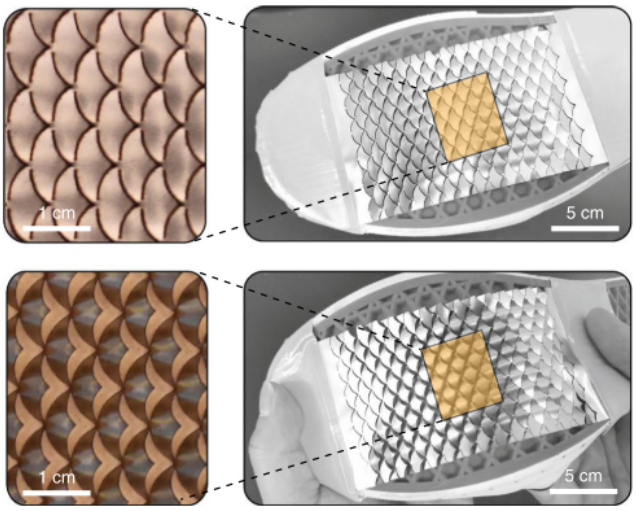

Fig. 28. Shoe grips that get more grip when the curvature of the sole changes, Babaee [1].

D. Real Hinges

O. Real hinges are used by Jasim [12], as a way to fold solar panels into a Miura-ori pattern (Fig. 29). This allows a large area to be folded compactly in one continuous motion. In this pattern, the facets are made of solar panels and they are connected by simple hinges. Due to the stiffness of the solar panels, combined with the strength of the hinges this technique can be used to create mechanisms in the meter range. Furthermore with the use of this technique the solar panel can be folded while following the theoretical kinematics. Another example is Torggler's Triangle door [29] (Fig. 30).

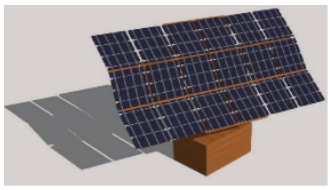

Fig. 29. A solar panel that can be folded in a Miura-ori pattern, Jasim [12].

This is a form of kinetic art where a door can be opened and closed by folding it. The wooden panels of the door are connected by hinges, this allows it to bend towards the open position. The door is around 1 by 2 meters, making it a large origami mechanism. This is again possible due to the stiff facets and strong hinges. Because of this the door also follows the theoretical kinematics, as the rigid panels will not deform. A kinetic sculpture is designed by Morgan [21] to demonstrate the offset panel technique (Fig. 31). This is a method within thick origami where thick panels are stacked next to each other when folded. The sculpture is made of one heavy base plate made of MDF, the rest of the facets are made of lighter foam board. These facets are all connected using hinges. The sculpture is more than a meter tall, making it a large origami

Fig. 30. Kinetic door by Torggler [29].

mechanism. This can be achieved due to the light foam board and strong hinges. The whole mechanism can be unfolded by pulling on only one of the panels. When this is done the mechanism becomes a flat plate, which means it follows the theoretical kinematics.

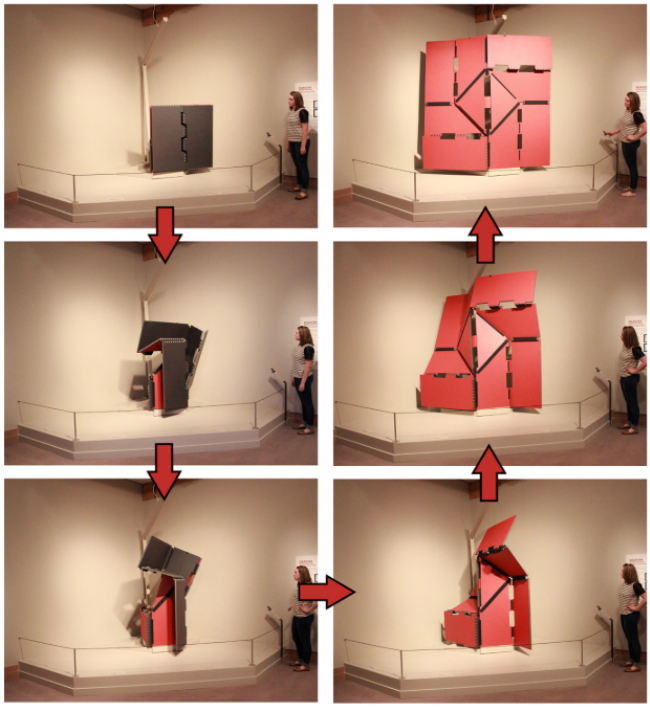

Fig. 31. Kinetic sculpture to demonstrate offset panels, Morgan [21].

IV. Discussion

By structuring the different ways people deal with achieving correct kinematics in origami mechanisms, it becomes clear that not all methods are effective. A method is deemed effective when the designed mechanism works as intended. Most papers that use a technique that reduces the crease stiffness need to combine this with a different method like *individual cell actuation* or *external constraints*. Together with these techniques, the mechanisms work as intended, and their kinematics follow the theory.

Another example of decreasing stiffness that does not work is seen in the origami-inspired metamaterial from Iniguez-Rabago [9]. In the theoretical model, eight stable states are present for the metamaterial, but in the prototype with thin hinges none of these states were stable. This is a clear example of the theoretical kinematics not being followed. After changing the thin hinges out with a more flexible material, six out of eight stable states were found in this prototype.

A clear size difference between methods also becomes apparent (Fig. 32). Decreasing crease thickness or width is used for rather small mechanisms in the centimeter range. These smaller mechanisms are in turn actuated using SMA or thermal expansion. When two different materials are used for the facets and the creases larger mechanisms can be constructed. These range from the centimeter scale up to the meter scale. The pneumatic and hydraulic actuation also allow for larger mechanisms. These mechanisms are generally in the decimeter range. The real hinges also stand out as this method is used for even larger mechanisms at the meter range. External constraints are an exception to this pattern and are found throughout all sizes, from micrometer to decimeter.

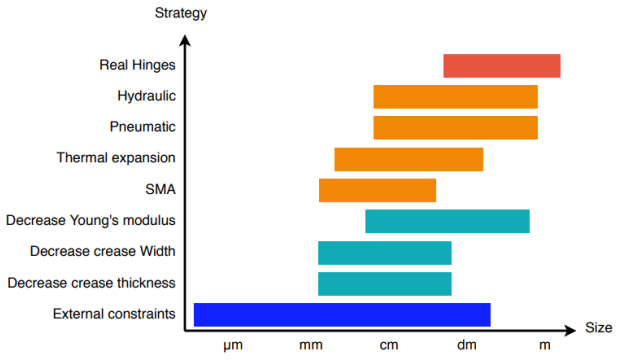

Fig. 32. Size differences between the strategies.

Finally, a research gap appeared, the use of prestress to decrease the stiffness of a crease has not been researched for origami mechanisms. However this does show potential from its application in compliant mechanisms.

V. Conclusion

In this survey, the techniques that improve the kinematics of origami mechanisms have been categorized and explained. In most papers regarding origami mechanisms, these techniques were not explicitly mentioned but were still present in the designs. The techniques are subdivided into four categories, *decreasing crease stiffness*, *individual cell actuation*, *external constraints*, and *real hinges*.

From this categorization was found that the current methods used to decrease the stiffness of the creases are not adequate for letting mechanisms follow their theoretical kinematics. A clear example of this was provided by the origami-inspired metamaterial that did not have any of its stable states when manufactured. But it could also be seen because mechanisms that relied on decreased crease stiffness were almost always combined with a technique from a different category. These combinations of techniques provided good kinematic behavior, but they also limited the possible applications of these mechanisms because often specific boundary conditions were applied, or an intricate actuation system was implemented. However, a research gap was found in prestressed creases that can accomplish static balancing. This technique has not been applied to origami mechanisms but could decrease the crease stiffness of a mechanism up to a point where the theoretical kinematics are followed.

Also, a clear picture of mechanism sizes originated from this categorization. Changing only the crease dimensions of a mechanism, such as thickness or width is suitable for small structures in the centimeter range. For structures in the decimeter range, it is more common to use a different material for the creases with a lower Young's modulus. This is the case because as a mechanism is scaled with a factor S, the stiffness of the crease scales with a factor S^3. So the bigger the mechanism becomes, the harder it is to create flexible creases. Using a material with a lower Young's modulus helps to create these flexible creases. This approach could also be used for the meter scale, just like the real hinges which are also best used at this scale. The real hinges are made of different parts and need assembling, on a small scale this can be tedious, but on a larger scale, this is easier. An added benefit is that the hinges do not have to be flexible and thus can be made as rigid as needed, this allows for heavier mechanisms to be possible. For the different actuation methods, SMA and thermal expansion can be used on a smaller scale. Because they are temperature-dependent increasing their size will also increase their response time, which is generally not wanted. For larger mechanisms, pneumatic and hydraulic systems can be used. These actuators can deliver enough force to actuate large mechanisms and can be easily scaled up if needed.

With the categorization in this literature survey, a clearer image is created of the techniques which are used to make origami mechanisms have proper kinematic behavior. This review can be used to help with the design of a kinematically correct mechanism, and it points out research opportunities for better performing techniques.

References

[1] Sahab Babaee et al. “Shoe Grips”. In: *Nature Biomedical Engineering* (). ISSN: 2157-846X. DOI: 10.1038/s41551-020-0564-3. URL: http://dx.doi.org/10.1038/s41551-020-0564-3.

[2] Michael S Baker and Larry L Howell. “On-Chip Actuation of an In-Plane Compliant Bistable Micromechanism”. In: 11.5 (2002), pp. 566–573.

[3] G Balaji et al. “An SMA-actuated , Compliant Mechanism-based Pipe-crawler”. In: (2008), pp. 1–9.

[4] Wojciech Bejgerowski et al. “Design and fabrication of miniature compliant hinges for multi-material compliant mechanisms”. In: *International Journal of Advanced Manufacturing Technology* 57.5-8 (2011), pp. 437–452. ISSN: 14333015. DOI: 10.1007/s00170-011-3301-y.

[5] Elisa Boatti, Nikolaos Vasios, and Katia Bertoldi. “Origami Metamaterials for Tunable Thermal Expansion”. In: *Advanced Materials* 29.26 (2017), pp. 1–6. ISSN: 15214095. DOI: 10.1002/adma.201700360.

[6] Ajit R. Deshpande, Zion Tsz Ho Tse, and Hongliang Ren. “Origami-inspired bi-directional soft pneumatic actuator with integrated variable stiffness mechanism”. In: *2017 18th International Conference on Advanced Robotics, ICAR 2017* July (2017), pp. 417–421. DOI: 10.1109/ICAR.2017.8023642.

[7] Regina M. Gouker et al. “Manufacturing of multi-material compliant mechanisms using multi-material molding”. In: *International Journal of Advanced Manufacturing Technology* 30.11-12 (2006), pp. 1049–1075. ISSN: 02683768. DOI: 10.1007/s00170-005-0152-4.

[8] Larry L. Howell. *Compliant Mechanisms*. Springer, London, 2013. ISBN: 978-1-4471-4510-3. DOI: https://doi.org/10.1007/978-1-4471-4510-3{_}7.

[9] Agustin Iniguez-Rabago, Yun Li, and Johannes T.B. Overvelde. “Exploring multistability in prismatic metamaterials through local actuation”. In: *Nature Communications* 10.1 (2019), pp. 1–10. ISSN: 20411723. DOI: 10.1038/s41467-019-13319-7. URL: http://dx.doi.org/10.1038/s41467-019-13319-7.

[10] Alexandra Ion et al. “Metamaterial mechanisms”. In: *UIST 2016 - Proceedings of the 29th Annual Symposium on User Interface Software and Technology* (2016), pp. 529–539. DOI: 10.1145/2984511.2984540.

[11] Alexandra Ion et al. “Metamaterial textures”. In: *Conference on Human Factors in Computing Systems - Proceedings* 2018-April (2018). DOI: 10.1145/3173574.3173910.

[12] Binyamin Jasim and Pooya Taheri. “An Origami-Based Portable Solar Panel System”. In: *2018 IEEE 9th Annual Information Technology, Electronics and Mobile Communication Conference, IEMCON 2018* 1 (2019), pp. 199–203. DOI: 10.1109/IEMCON.2018.8614997.

[13] Magnus H. Kaspersen et al. “Lifting Kirigami Actuators up where they belong: Possibilities for SCI”. In: *DIS 2019 - Proceedings of the 2019 ACM Designing Interactive Systems Conference* (2019), pp. 935–947. DOI: 10.1145/3322276.3323688.

[14] Jongwoo Kim et al. “A self-deployable origami structure with locking mechanism induced by buckling effect”. In: *Proceedings - IEEE International Conference on Robotics and Automation* 2015-June.June (2015), pp. 3166–3171. ISSN: 10504729. DOI: 10.1109/ICRA.2015.7139635.

[15] Kaori Kuribayashi et al. “Self-deployable origami stent grafts as a biomedical application of Ni-rich TiNi shape memory alloy foil”. In: *Materials Science and Engineering A* 419.1-2 (2006), pp. 131–137. ISSN: 09215093. DOI: 10.1016/j.msea.2005.12.016.

[16] Shuguang Li et al. “A Vacuum-driven Origami “ Magic-ball ” Soft Gripper”. In: (2019), pp. 7401–7408.

[17] Shuguang Li et al. “Fluid-driven origami-inspired artificial muscles”. In: *Proceedings of the National Academy of Sciences of the United States of America* 114.50 (2017), pp. 13132–13137. ISSN: 10916490. DOI: 10.1073/pnas.1713450114.

[18] Suyi Li and K. W. Wang. “Fluidic origami: A plant-inspired adaptive structure with shape morphing and stiffness tuning”. In: *Smart Materials and Structures* 24.10 (2015). ISSN: 1361665X. DOI: 10.1088/0964-1726/24/10/105031.

[19] Zhaowen Lin et al. “Folding at the Microscale: Enabling Multifunctional 3D Origami-Architected Metamaterials”. In: *Small* 2002229 (2020), pp. 1–9. ISSN: 16136829. DOI: 10.1002/smll.202002229.

[20] Ezekiel G. Merriam, Kyler A. Tolman, and Larry L. Howell. “Integration of advanced stiffness-reduction techniques demonstrated in a 3D-printable joint”. In: *Mechanism and Machine Theory* 105 (2016), pp. 260–271. ISSN: 0094114X. DOI: 10.1016/j.mechmachtheory.2016.07.009. URL: http://dx.doi.org/10.1016/j.mechmachtheory.2016.07.009.

[21] Michael R. Morgan et al. “Towards developing product applications of thick origami using the offset panel technique”. In: *Mechanical Sciences* 7.1 (2016), pp. 69–77. ISSN: 2191916X. DOI: 10.5194/ms-7-69-2016.

[22] Cagdas D. Onal, Robert J. Wood, and Daniela Rus. “An origami-inspired approach to worm robots”. In: *IEEE/ASME Transactions on Mechatronics* 18.2 (2013), pp. 430–438. ISSN: 10834435. DOI: 10.1109/TMECH.2012.2210239.

[23] Johannes T.B. Overvelde et al. “A three-dimensional actuated origami-inspired transformable metamaterial with multiple degrees of freedom”. In: *Nature Communications* 7 (2016), pp. 1–8. ISSN: 20411723. DOI: 10.1038/ncomms10929.

[24] M. R.Aravind Raghavendra, A. Senthil Kumar, and Bhat Nikhil Jagdish. “Design and analysis of flexure-hinge parameter in microgripper”. In: *International Journal of Advanced Manufacturing Technology* 49.9-12 (2010), pp. 1185–1193. ISSN: 02683768. DOI: 10.1007/s00170-009-2478-9.

[25] Mark Schenk and Simon D. Guest. “Geometry of Miura-folded metamaterials”. In: *Proceedings of the National Academy of Sciences of the United States of America* 110.9 (2013), pp. 3276–3281. ISSN: 00278424. DOI: 10.1073/pnas.1217998110.

[26] M. Sreekumar, T. Nagarajan, and M. Singaperumal. “Application of trained NiTi SMA actuators in a spatial compliant mechanism: Experimental investigations”. In: *Materials and Design* 30.8 (2009), pp. 3020–3029. ISSN: 02641275. DOI: 10.1016/j.matdes.2008.12.017. URL: http://dx.doi.org/10.1016/j.matdes.2008.12.017.

[27] Cynthia Sung and Daniela Rus. “Foldable joints for foldable robots”. In: *Journal of Mechanisms and Robotics* 7.2 (2015), pp. 1–13. ISSN: 19424310. DOI: 10.1115/1.4029490.

[28] Tomohiro Tachi, Motoi Masubuchi, and Masaaki Iwamoto. “Rigid Origami Structures with Vacuumatics : Geometric Considerations”. In: *Proceedings of the IASS-APCS 2012* (2012), p. 8.

[29] Klemens Torggler. *Triangle door*. 2016.

3

Paper: Design of a constant moment crease for use in neutrally stable origami

DESIGN OF A CONSTANT MOMENT CREASE FOR USE IN NEUTRALLY STABLE ORIGAMI

Edward van Wijk

ABSTRACT

Origami mechanisms are mechanisms that are inspired by the art of origami. They have the potential to be used in different applications. However, a problem is that the stiffnesses of their creases introduce unwanted artifacts. Such as larger actuation forces, and a lack of proper kinematics. In this paper, a constant moment crease is designed, which can be used to statically balance an origami mechanism, that way removing its stiffness. The crease has a convex shape and has two corrugated facets on its sides. The constant moment is realized through modeling the crease in a FEM program and optimizing it for a constant moment. This model is validated by a prototype experiment. The result of the paper is a crease that has a constant moment over a range of 80°.

1 Introduction

Origami is a technique where structures are created by folding flat sheets. This is best known from artworks but it is also interesting for engineers. Origami has become a source of inspiration for engineers. This is because it is scalable, and has the potential to switch between different states. This makes it applicable in many fields [1]. Therefore more and more research is being done into origami mechanisms. A problem with origami mechanisms is that the stiffness of the creases introduces artifacts into the system which are not wanted [2]. For example, the actuation force increases when the mechanism is actuated. Another problem is that the kinematics of an origami pattern do not follow the theory anymore. In theory, every cell in an origami pattern should have the same deformation, but if there is stiffness in the mechanisms, the actuated cell will be the most deformed, and the cells connected to it will not be deformed as much. There are multiple ways that researchers use to negate these artifacts, most are aimed at decreasing the crease stiffness in the mechanism. This can be done by decreasing the crease thickness [3, 4], perforating the crease [5], or decreasing the Young's modulus of the crease [6–8]. But using these strategies will never give a truly zero stiffness crease.

A zero stiffness mechanism could be achieved with the concept of static balancing. This is a concept where two different elements are combined to balance each other. If these two elements are combined in parallel, their moment-angle characteristics are summed up. If this sum equals zero over a certain range, the system is statically balanced in the domain of this range.

This can be achieved by balancing an element with a flat moment-angle characteristic with a mirrored version of itself. These two elements need to be prestressed into the right position such that the constant moment regions overlap, this will result in a statically balanced mechanism. This is demonstrated by Radaelli [9] for multiple mechanisms such as a four- or six-bar linkage. Compliant mechanisms with a constant moment have already been designed, two examples are by Hou, [10] and Gandhi, [11]. With a constant moment crease and static balancing, the stiffness of the creases in an origami mechanism could become truly zero.

However, this previous research does not focus on origami mechanisms, therefore, these constant moment mechanisms are difficult to implement into an origami pattern. Tape springs have also been shown to exhibit a constant moment during bending [12, 13]. This could have a potential for origami, but this technique is not optimal. Firstly, a tape spring is usually longer than that it is wide, whereas a crease is usually wider than that it is long. And secondly, there is not an exact point where the tape spring bends, because it has the same cross-section over its whole length.

In this paper, a constant moment crease is designed, which has a constant moment over a relevant range of motion for an origami mechanism. The crease is a convex

shape and this convexity is gradually reversed when the crease is bending. This crease is modeled in a FEM program, together with two corrugated facets attached to it. This model is then validated by a prototype experiment.

In the methods section, the approach to find a constant moment crease is explained. The model and optimization are discussed, as well as the test setup. This is followed by the results where both the obtained moment-angle characteristics of both the model and the prototype experiment can be found. In the discussion, it is explained what the results look like and why this is the case. Together with how the creases could be implemented into an origami pattern. Finally, a conclusion on the performance of the creases is drawn from this discussion.

2 Methods

2.1 Neutrally stable origami

How a constant moment crease can be used to make origami neutrally stable is explained on the basis of a Miura-ori tesselation, which is a pattern of identical origami cells. In FIGURE 1, a schematic of the creases of one Miura-ori cell can be seen. The solid lines represent mountain folds, these creases are folded upwards. The dashed lines represent valley folds, these creases are folded downwards. Multiple of these cells can be chained together to make a Miura-ori tessellation. There is an equal number of mountain and valley folds in every unit cell. This means that the number of creases folding upwards is equal to the number of creases folding downwards. This allows balancing every valley fold with its opposite mountain fold.

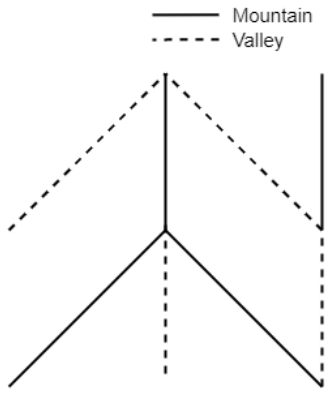

FIGURE 1: Schematic of Miura-ori fold lines, the amount of mountain and valley creases is equal.

If a fold line has a constant moment this needs to be balanced by an opposite constant moment of equal magnitude. The same crease can be used for this so that the constant moment is equal for both creases. To make the constant moment of one crease oppose the constant moment of another crease they need to bend in opposing directions, so one crease should bend clockwise while the other bends counterclockwise. Because in this method mountain and valley folds are balanced, all the creases can be placed the same side up. Because half of the creases bend into a mountain and the other half into a valley, as many creases will bend clockwise as counterclockwise, this will give the needed effect of opposing moments. One final step needed to achieve this is the pre-stressing into the constant moment area. This can be done by bending the crease until it reaches its constant moment region and assembling it in that configuration into the Miura-ori pattern.

2.2 Concept

The design of a constant moment crease starts with a predetermined shape. This shape consists out of a convex crease with a positive Gaussian curvature, which has corrugated facets on both sides (FIGURE 2). The convex shape

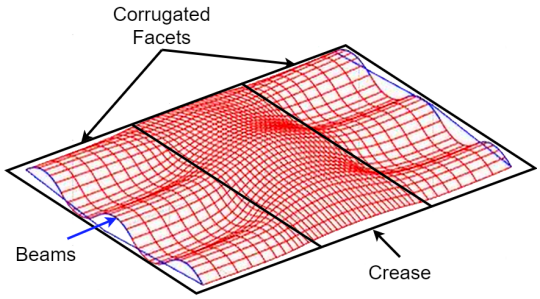

FIGURE 2: Shell concept with a convex crease and corrugated facets

was chosen because its positive Gaussian curvature has potential for bi-stable behavior, like a push bubble toy that can be turned inside out. This bi-stability however only exists for very thin shells, with thicker shells the stiffness of the material will add to the stiffness of the geometry and the negative stiffness will be replaced by zero stiffness. So a not-too-thin ellipsoid-shaped shell has the potential to create a constant moment. The facets are implemented into the design so it is possible to look at the behavior of the crease in combination with the facets. This makes the results more similar to how they would perform in an actual origami pattern. A corrugation is chosen to give the facets more stiffness than the crease while simultaneously keeping the thickness of both the facets and the crease the same.

2.3 Simulation

To check if this shape will have a range with a constant moment, it is numerically modeled with an isogeometric analysis framework [14]. This is based on the Kirchhoff-Love plate theorem and a linear isotropic material law. A geometry can be modeled by describing it in several control points. The code will fit a B-spline, which is attracted to these control points, this will result in a surface, which is given a thickness to create a shell. The control points of the facets are defined by the parameters from Table 1 and FIGURE 3. The corrugations are equally spaced along the length of the shell, and the ends taper off to the side of the crease. The control points of the crease are arranged in a 3x7 grid, and all lie on an ellipsoid. This ellipsoid is located between the two facets and is defined by a rectangle that is made up by the crease width and the length, the ellipsoid height, and a scaling factor in y-direction. The ellipsoid is drawn through the four corners of the rectangle, with the ellipsoid height being the distance in z-direction between the corners of the rectangle and the highest point on the ellipsoid. Finally, a scaling factor is used to define the circularity of the ellipsoid. This scaling factor scales the radius of the ellipsoid in y-direction compared to the radii in x- and z-direction.

The resulting shell can be seen in red in FIGURE 2. Onto the sides of the shell beams are added, these are shown in blue. These beams have a stiffness multiple orders of magnitudes higher than the stiffness of the shell itself. These mostly follow the side profile of the shell, but two beams are drawn from the edges of the shell to the middle, only offset by 5 mm in the x-direction. These two points are known as pilot points. these are the points that the constraints are applied to, and because the beams are multiple orders stiffer than the shell, these constraints are passed on to the edge of the shell. The shell is bend by rotating one of the pilot points around the y-axis and constraining its other degrees of freedom. Then the second pilot point is constrained in z-translation, this allows it to rotate and move closer to the other axis.

To find a constant moment, a sensitivity analysis of the parameters from TABLE 1 was done. All the parameters were fixed to a constant value except for one, this parameter was varied. For each different value of this parameter, a simulation was run, and from this, the moment-angle characteristic was plotted. This way it was possible to see which parameter influenced the shell in such a way that it exhibited a constant moment.

From this approach, three different geometries were found that showed initial signs of a constant moment. For these three geometries, the thickness of the shell was also varied. The FEM code also provides an animation of the deformation of the shell, this can give more insight into why

W_f	Flange width
W_t	Taper width
W	Crease width
L	Length
H_c	Corrugation height
H_e	Ellipsoid height
S_y	Scaling factor of ellipsoid in y-direction

TABLE 1: Parameter definitions

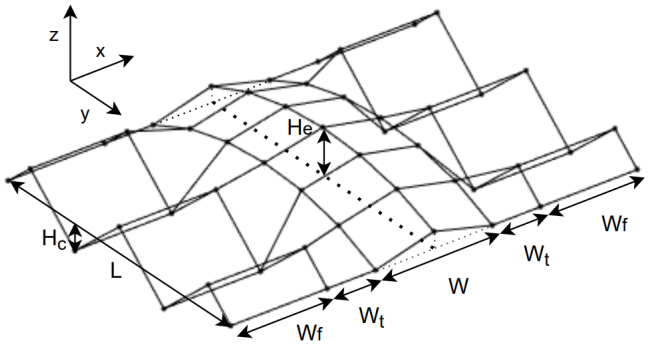

FIGURE 3: Parameters that define the control points of the geometry

the moment-angle characteristic looks like it does. With the initial results that show a potential for a constant moment crease, a further search can be done to find a moment-angle characteristic with better performance. This performance is based on two factors, the flatness of the characteristic and the range of motion over which this flatness is present. This is achieved by using an optimization algorithm, this algorithm varies multiple variables at each iteration to find the lowest value for an objective function. By setting the flatness between two points as the objective, the algorithm will find the flattest curve possible within the given parameters. The flatness of the interval is defined as the normalized Root Mean Square Error (RMSE) with respect to the average moment on that interval. First, this average moment is calculated using equation 1. Here n is the number of data points on the interval. With this average, the RMSE and normalized RMSE are calculated according to equations 2 and 3.

$$\hat{M} = \frac{\sum_{i=1}^{n} M_i}{n} \tag{1}$$

$$\text{RMSE} = \sqrt{\sum_{i=1}^{n} \frac{\left(\hat{M} - M_i\right)^2}{n}} \tag{2}$$

$$\text{Normalized RMSE} = \frac{\text{RMSE}}{\hat{M}} \tag{3}$$

There are three variables that the algorithm can use to minimize the Normalized RMSE: W, S_y, and H_e. These variables allow for the ellipsoid part to change in shape, while the facets will keep their shape. This is chosen because previous results showed that the shape of the ellipsoid has more influence on the moment-angle characteristic than the shape of the facets. Also, by keeping the numbers of variables low the calculation time of the optimization will stay short. The optimization algorithm used is the fminsearch algorithm from the MATLAB optimization toolbox, aside from variables and an objective this algorithm also needs a starting point. For this, the best results from the previous modeling stage were used. Because the objective function only takes into account the flatness of the moment-angle characteristic, the range of this flatness needs to be specified as well. Running this optimization will only provide the flattest option within the specified range. To increase the range over which a constant moment is present, the optimization range is manually increased after each optimization run, with the result of each previous smaller range as a starting point for the search of a larger range. When the optimization algorithm can no longer find a constant moment over the whole range the range will no longer be increased.

For a second optimization, the crease definition was changed. The control points of the crease are no longer defined by an ellipsoid. The control points still consist out of a 3 by 7 grid, however, the heights of the seven points through the middle are defined by four independent parameters, namely H1, H2, H3, and H4. The height of the points on the side is dependent on the height of their adjacent point, and scaled by a scale factor S. This is visualized in FIGURE 4. Because the heights of the middle control points are independent of each other the optimization algorithm has more freedom to choose different shapes. This offers more flexibility compared to the ellipsoid definition of the previous optimization.

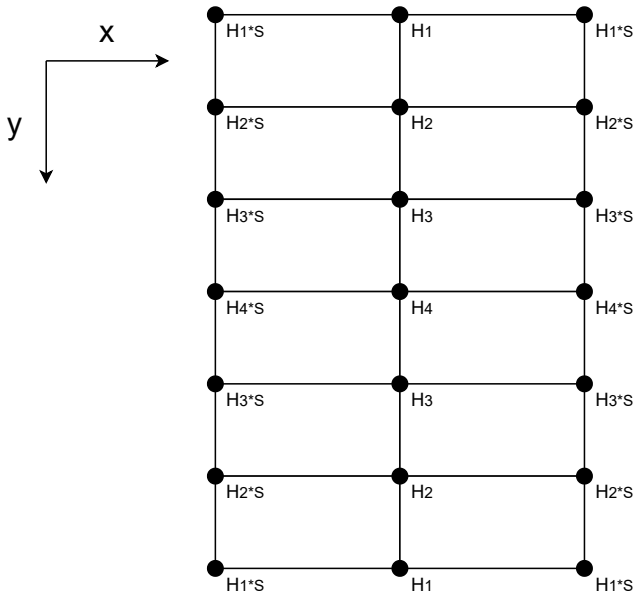

FIGURE 4: 2D representation of new optimization parameters

2.4 Prototype experiment

Next to the modeling, there was also an experimental validation performed. This was done to validate if the modeled data represents the shell in reality. For this, the same constraints are needed as used in the model. This was realized with the test setup in FIGURE 5. The shell is 3D-

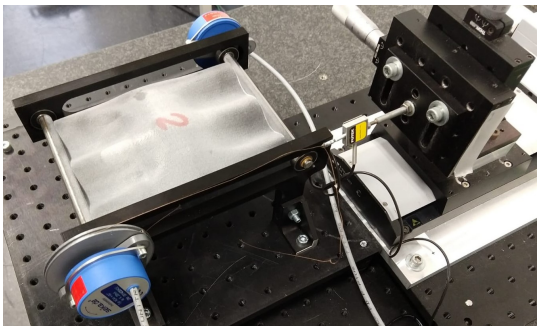

FIGURE 5: Test setup with a force sensor connected via a wire to the pulley, and two inclinometers fixed onto the axes

printed using multi-jet fusion, made of the material PA 12. Two steel axes are glued onto the shell, at the point where the rigid beams were modeled. One of the axes is only allowed to rotate, it is constrained by two ball bearings in a frame. The other axis is only constrained in the z-direction, this is achieved by connecting two ball bearings to the axis

and allowing those to roll in a slot. A pulley is mounted on the first axis, to which a braided steel wire is connected and rolled around. By pulling on the wire, the pulley is rotated and a moment is applied to the axis. The force in the wire is measured with a FUTEK Miniature S-Beam Jr. Load Cell LSB200, with a maximum force of 45N. The angles of both axes are measured with two separate SEIKA NG4i inclinometers, which can measure an angle up to 160°. These are connected to the axes. The wire can be pulled mechanically on a test bench, this ensures a constant rotation of the pulley, which gives a repeatable result.

Six shells with the same geometry were used in the experiment. Three of these were 3D-printed with a thickness of 0.4 mm, and the other three with a thickness of 0.5 mm. However, there was a variation of thickness in the prototypes. The different thicknesses of the shells are shown in TABLE 2. These values are an average of multiple measurements with a micrometer. A micrometer is designed to measure a flat object between its flat spindle and anvil. Because the prototypes are curved two bearing balls were connected to the spindle and anvil of the micrometer, this allowed for measurements of the curved surface. The average thickness of the three thicker shells is 0.66 mm, and for the three thinner shells this is 0.57 mm. These values are used in the model for a moment-angle characteristic that can be compared to the experiment result. For this comparison, the model also needs the Young's modulus of the material. For this, a Young's modulus of 900 MPa was used.

Prototype	1	2	3	4	5	6
Thickness [mm]	0.675	0.660	0.632	0.578	0.577	0.562

TABLE 2: Thickness of the prototypes, a difference between two print thicknesses can be seen, but the thicknesses are still varied

3 Results

In this section results of the modeling, and the results of the prototype experiment are shown. This is ordered into the three different geometries that showed a constant moment. With the sensitivity analysis, one variable was found for each geometry that showed a constant moment behavior, this is shown in the first FIGURES: 7a, 8a, and 10a. In the same figures, a variation of the thickness of the entire shell is also shown, FIGURES: 7b, 8b, and 10b. This is followed by the result of the optimization combined with a depiction of the different states of the shell, FIGURES: 6, 9, and 11. In these figures, an orange line is plotted, this indicates the range over which the optimization was performed. The dimensions of the facets are the same for all simulations and can be found in TABLE 3. Here also the dimensions of the initial geometries of the creases are shown. The dimensions of the optimized geometries can be found in TABLE 4, together with the achieved range of motion where there is a constant moment, and the normalized root mean square error, which represents the flatness of the constant moment.

Facets	$\mathbf{W_f}$ [mm]	$\mathbf{W_t}$ [mm]	**L** [mm]	$\mathbf{H_c}$ [mm]
	40	10	120	10
Crease	**W** [mm]	$\mathbf{H_e}$ [mm]	$\mathbf{S_y}$ [-]	**t** [mm]
FIGURE 7a	50	varied	2	0.5
FIGURE 7b	50	6	2	varied
FIGURE 8a	100	varied	2	0.5
FIGURE 8b	100	30	2	varied
FIGURE 10a	varied	15	2	0.5
FIGURE 10b	40	15	2	varied

TABLE 3: Geometry 1 parameter dimension in meters

For Geometry 3 a prototype experiment was performed, the results of which are split into two graphs. FIGURE 12 shows the moment-angle characteristic of the model together with the hysteresis loops of the three thicker prototypes. FIGURE 13 shows the moment-angle characteristic of the model together with the hysteresis loops of the three thinner prototypes.

	$\mathbf{H_1}$ [mm]	$\mathbf{H_2}$ [mm]	$\mathbf{H_3}$ [mm]	$\mathbf{H_4}$ [mm]	**S** [-]	$\mathbf{W_t}$ [mm]	RoM [deg]	Error [-]
FIGURE 6	1.6	5.4	6.5	5.6	0.67	20.0	15	0.013
FIGURE 9	19.8	32.7	38.3	24.4	0.67	20.0	50	0.024
FIGURE 11	5.4	11.8	13.0	18.9	0.67	20.0	80	0.048

TABLE 4: Parameter dimensions for the second optimization in meters

3.1 Geometry 1

Here the results of the first geometry are shown. First, in FIGURE 7a, a variation of the height of the ellipsoid is shown. At a height of 6 mm a constant moment appears between 10° and 25°. Then in FIGURE 7b, a variation of the thickness of the shell is displayed. In FIGURE 6, the optimized moment-angle characteristic can be seen together with the different states the shell is in. The numbers of the states correspond to the numbered positions on the moment-angle characteristic. Here there also is a constant moment between 10° and 25°.

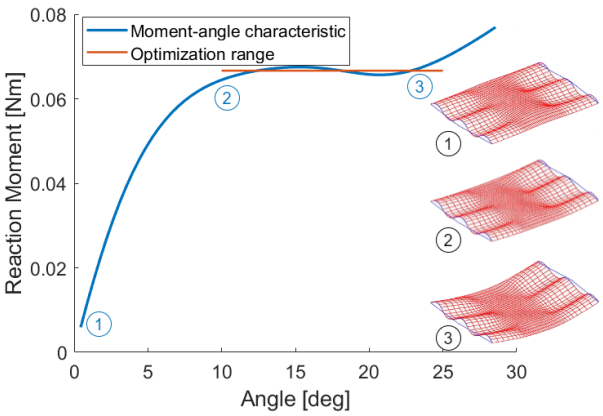

FIGURE 6: Optimization of the first geometry with deformation states, there is a constant moment between 10° and 25°

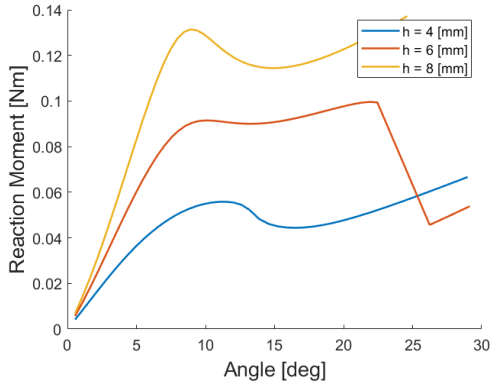

(a) Moment-angle characteristics with varying convexity, which shows an almost constant moment for h = 6 mm

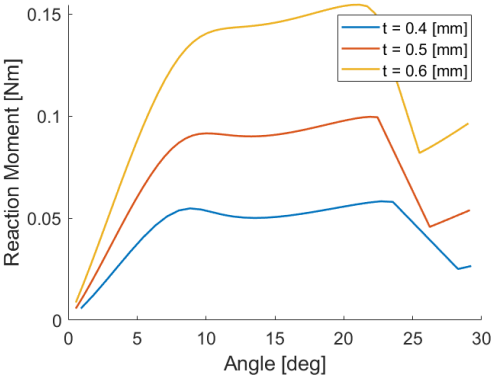

(b) Moment-angle characteristics for varied thicknesses, the thicker shells have a higher moment and stiffness

FIGURE 7

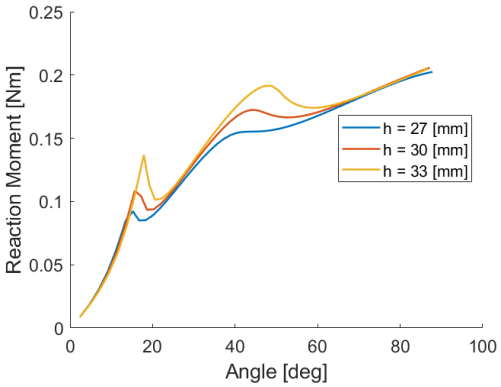

(a) Moment-angle characteristics with varying convexity, around 50° a positive stiffness changes to a negative stiffness, this indicates that a constant moment can be achieved

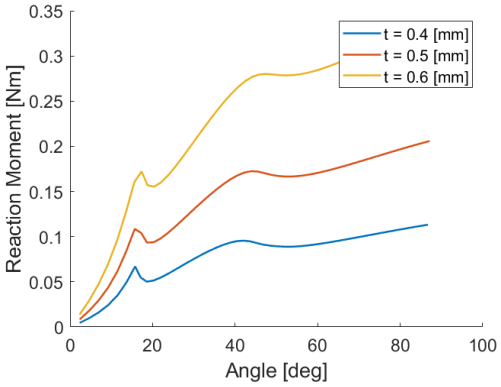

(b) Moment-angle characteristics for varied thicknesses, the thicker shells have a higher moment and stiffness

FIGURE 8

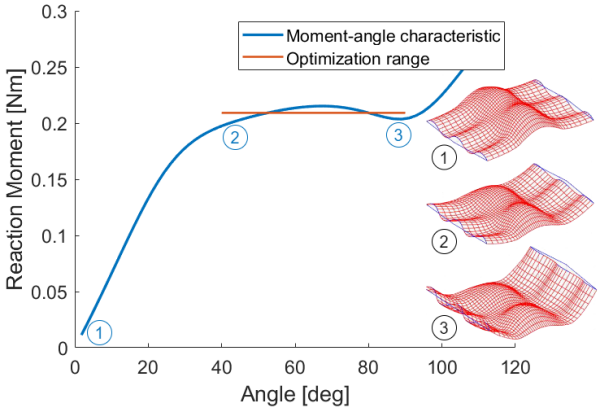

FIGURE 9: Optimization of the second geometry with deformation states, there is a constant moment between 40° and 90°

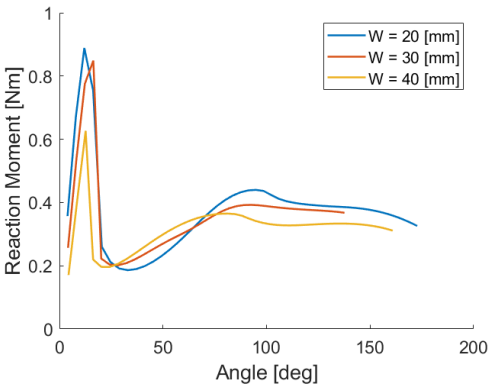

(a) Moment-angle characteristics with varying width, a constant moment appears around 100°

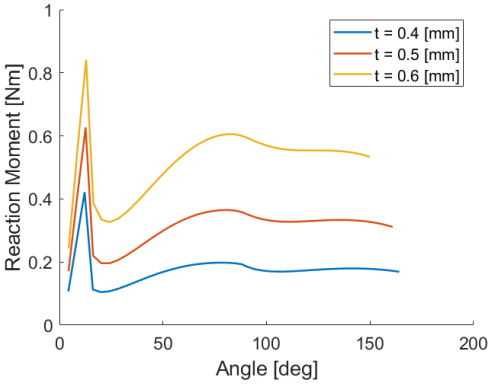

(b) Moment-angle characteristics for varied thicknesses, the thicker shells have a higher moment, but a lower stiffness on the constant moment range

FIGURE 10

3.2 Geometry 2

Here the results of the second geometry are shown. First, in FIGURE 8a, a variation of the height of the ellipsoid is shown. At a height of 30 mm a constant moment appears between 45° and 60°. Then in FIGURE 8b, a variation of the thickness of the shell is displayed. In FIGURE 9, the optimized moment-angle characteristic can be seen together with the different states the shell is in. The optimization gives a constant moment between 40° and 90°.

3.3 Geometry 3

Here the results of the third geometry are shown. First, in FIGURE 10a, a variation of the width of the crease is shown. At a width of 40 mm, a constant moment appears. Then in FIGURE 10b, a variation of the thickness of the shell is displayed. In FIGURE 11, the optimized moment-angle characteristic can be seen together with the different states the shell is in. This optimization gives a constant moment between 80° and 160°.

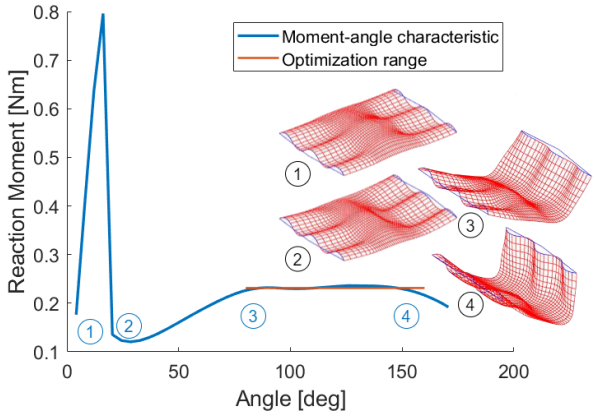

FIGURE 11: Optimization of the third geometry with deformation states, there is a constant moment between 80° and 160°

3.4 Prototype experiment

In FIGURE 12, the measured moment-angle characteristics of the three thicker shells are shown together with the moment-angle characteristic of the model with a thickness of 0.66 mm, which is the average thickness of the three prototypes. The measured hysteresis loops show a similar shape to the curve predicted by the model. In FIGURE 13, the measured moment-angle characteristics of the three thinner shells are shown together with the moment-angle characteristic of the model with a thickness of 0.57 mm, which is the average thickness of the three prototypes. Two of these shells were too thin to fully deform back, this is why their hysteresis loops end at 43° and 56°, instead of 0°. The shapes of the hysteresis loops are similar to the curve predicted by the model.

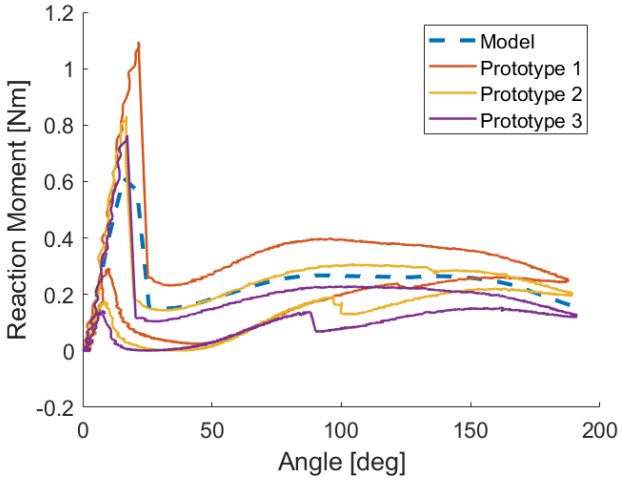

FIGURE 12: Hysteresis loops of the three thicker shells, they have a similar shape to the moment-angle characteristic of the model

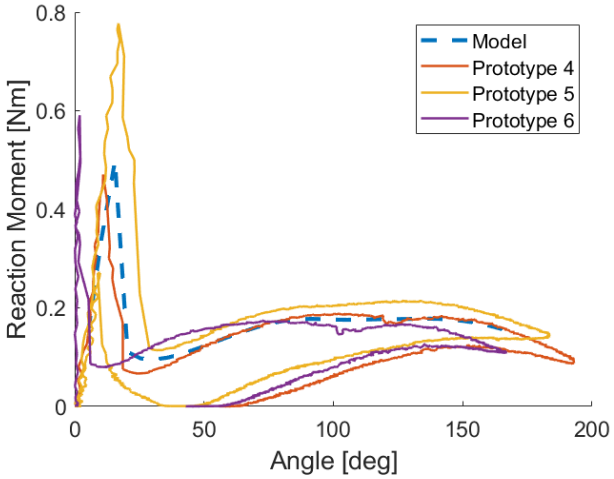

FIGURE 13: Hysteresis loops of the three thinner shells, they have a similar shape to the moment-angle characteristic of the model

4 Discussion

From the results section, three different geometries were found that can work as a constant moment crease. The findings are discussed below per geometry. The results of the prototype test and the implementation of the crease into origami are discussed separately.

4.1 Geometry 1

By tuning the height of the crease to the right parameter a constant moment appears for this geometry. The crease is only slightly convex compared to the other geometries. By reducing the thickness of the overall shell the moment is decreased, but the stiffness which is the slope of the moment is decreased as well. This is expected because a thinner shell has a lower bending stiffness.

The optimization gives a shorter range of motion than the other geometries, but the error is also smaller, so the moment is more constant. The range of motion could be increased, but that will make the error go up more, and the moment becoming less constant. The crease of the optimized shape does not resemble the ellipsoid anymore. The middle point on the shell is actually lower than its neighboring points, just like in geometry 2. The deformation states show what the shell looks like at different points on the moment-angle characteristic. At point 2 the middle ridge of the right facet forces the crease into a snapped state around this ridge. This gives a valley around the middle ridge. This valley expands over the whole length of the crease. After this at point 3, the whole crease snaps into a valley. The first snapped state and the expansion over the length of the crease can be more clearly seen in the third geometry (FIGURE 11), because it is more convex. The constant moment occurs while the valley is expanding along the crease.

4.2 Geometry 2

In the second geometry, a wider and more convex crease is used. By varying the convexity, the moment-angle curve transitions from a positive stiffness to a negative stiffness, around the 50° to 60° mark. This implies that somewhere between these curves a constant moment can be found. Like with the first geometry, an increase in the thickness will increase the moment and the stiffness of the curve. This could be used to balance out the negative stiffness part of the curve, as the negative stiffness is mainly a result of the shape. By increasing the thickness, the positive stiffness of the shell is increased and balances out the negative stiffness of the shape.

Compared to the first geometry, the optimization yields a longer range of motion, but its error is bigger. The range of motion can be expanded but this would be done at the cost of the constant moment. This can be explained due to the sine shape of the curve. A perfect constant moment can only be achieved for an infinitesimally small interval. When optimizing this geometry on a larger interval the best solution will still be a sine wave. And the larger the optimization range the larger the amplitude of this sine wave needs to be to cover the entire range. Just like geometry 1, there is no sign of an ellipsoid anymore in the optimized shape. The middle point of the crease is again lower than its neighboring points. From the deformation states, it is difficult to see what happens with the shell that provides the constant moment. There are no parts of the shell that buckle or snap into a new position like with geometry 1. Therefore it can be assumed that due to the bending deformation, the geometry changes in such a way that the bending moment stays constant.

4.3 Geometry 3

Finally, a shell with a crease height that is in between the previous two was modeled. Here the width of the crease was varied which resulted in a constant moment between 100° and 160°. Similar to the previous geometries, a higher thickness also means a higher moment. However, the stiffness at the constant moment range seems to decrease with a higher thickness, the stiffness at the range before that behaves as expected and increases with the crease thickness. Why the stiffness decreases on the constant moment range will be discussed further down.

The optimized range with a constant moment is even larger than geometry 2. But the error is also larger. In FIGURE 11, the states of the shell during deformation can be found. Like with geometry 1, the middle ridge snaps the crease (point 2), and the valley that originates from that, spreads across the length of the crease. This leaves a ridge and a valley next to each other (point 3). When the shell is bent further, the valley grows. The valley appears to become flatter, this decreases the moment that is needed to bend the geometry. After this, the ridge is being pushed away completely by the valley, which increases the moment again. At point 4 the ridge is completely displaced by the valley.

In FIGURE 14, the moment-angle characteristic of a flat crease between the corrugated facets is shown. First, there is a positive stiffness and the moment needed to bend grows. This is what is expected when bending a flat crease. However, after bending 135° the stiffness becomes negative, and the moment decreases. This can be explained due to how the model is constrained. The moment on the driving axis is balanced by a normal force on the other axis. When the shell is bent, these axes get closer to each other, shortening the arm on which the normal force works. This decreases the moment and causes negative stiffness. To get a constant moment, the geometry should first add a negative stiffness part, and then after 135° a positive stiffness part. This is also what happens in the shell, as described above. Which causes the constant moment. The effect of the constraints can also explain the decreasing stiffness at a higher thickness. A thicker shell will also need a higher moment to deform, which causes a higher reaction force.

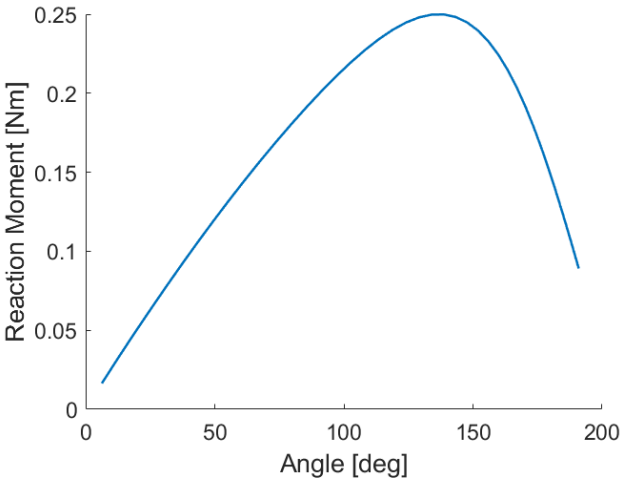

FIGURE 14: Moment-angle diagram of a flat crease between corrugated facets, at first it has a positive stiffness, but after 135°, it has a negative stiffness

This means that when the arm becomes shorter the negative stiffness is steeper due to the higher reaction force.

4.4 Prototype experiment

The characteristics of the prototype follow the curve of the model, which validates that the model correctly calculates the moment-angle characteristics of the crease. The magnitudes are also comparable, however, this is because the right Young's modulus in the model was chosen to achieve this. The Young's modulus of 3D printed PA 12 can be variable and is also dependent on the printing direction. A study by O'Connor [15] showed a Young's modulus around 1200 MPa. In the model, a Young's modulus of 900 MPa was used. This is significantly lower, but it gave a fitting curve for two different thicknesses. This means that the model can give the proper moment-angle characteristic when tuned correctly.

The thickness differed per tested shell, this explains the difference in moment between the prototypes. Two shells were too thin to fully deform back after bending. They reached a second stable point, and the shell was not stiff enough to push through that point. The other four shells did not have this problem.

What can also be seen is that the thickest shell, Prototype 1, shows a negative stiffness instead of a constant moment. This was also observed during the parameter study when the thickness of the shell was varied. Here a thicker shell caused more negative stiffness.

An inconsistency with the model is found for prototypes 2 and 3. While bending back to the initial position the shell snaps which causes a step in the curve around 100°. This only happened in these two shells so it is likely that this is caused by a difference in the production of the shells. Another inconsistency with the model is the hysteresis. During the bending of the shell, the needed moment is higher than when the shell is bent back. To verify if this hysteresis comes from the test setup, the shell was replaced by a 1 kg mass that was suspended from the pulley. This yielded a hysteresis loop with two constant moment lines, one for pulling the weight up and one for letting it back down. The lower moment line was at a height of 99% of the upper moment line. So only a small amount of hysteresis can be attributed to the test setup. This indicates that the hysteresis is inherent to the shell itself.

4.5 Implementation into origami

With the achieved constant moment of the crease, it could be implemented into an origami pattern to make it neutrally stable. The range of this neutral stability can be up to 80°. This however would only work for origami mechanisms where the creases have similar boundary conditions as the model, so a moment on one side of the crease, and a height constraint on the other side. If geometry 2 is used, a range of motion of 50° can be achieved. For different boundary conditions, the geometry needs to be optimized again. This became apparent by running the model with a moment constraint on both pilot points. The moment-angle characteristics of geometries 1 and 2 look similar to the characteristics that were initially found in the sensitivity analysis. So with a new optimization step, it should be possible to achieve a constant moment with different boundary conditions. This optimization was also performed which again resulted in two constant moment creases. Using the same constraints for geometry 3 gives a moment angle characteristic with a positive stiffness on the range where there was previously a constant moment. This is expected because the previous constraints contribute to the negative stiffness. Without this negative stiffness from the constraints, there is no longer a constant moment. It will also be difficult to regain a new constant moment with another optimization because the entire negative stiffness component should come from the geometry, instead of the boundary conditions. It was also tried to optimize this geometry for these other boundary conditions. This did indeed not result in a constant moment crease.

Pre-stressing can be made easier with this design by putting the facets on an angle relative to the crease, then if this is the correct angle, the facets can be straightened and the crease will reach its constant moment region. Putting the facets on an angle should not influence the behavior of the crease as long as the connection between the facets

and the crease is kept the same. With such a neutrally stable origami pattern the theoretical stiffness ratio between the facets and the crease is infinite. This means that the origami pattern will move according to the theoretical kinematics of the rigid origami concept [16], which will make origami mechanisms more predictable and easier to design, as their movements are just a matter of kinematics. Furthermore, moving neutrally stable mechanisms does not require any energy, this means that these mechanisms can be more efficient than non-balanced mechanisms.

5 Conclusion

In this paper, three designs of a constant moment crease were shown, each with its own constant moment range. Also, a model was developed that optimizes these creases for a constant moment. And this model was validated by a prototype experiment. Although the constant moments of the found geometries are dependent on the boundary conditions of the crease, this should not be a problem, because the model can be used to optimize the creases for different boundary conditions. The prototype experiment showed that there is hysteresis in the shells, this makes the shells difficult to use for a static balancing purpose because this assumes that the moment-angle characteristic is a line and not a loop. This problem can be solved by fabricating the crease out of a material that does not show hysteresis.

For implementation into origami mechanisms, either the second or third geometry is the most feasible. The third geometry can provide a range of motion up to 80°, which makes it suitable for more applications. However, because its constant moment depends heavily on the constraints of the mechanism, it can only be applied to a mechanism with similar constraints to what was used for the model. The second geometry on the other hand has with 50° a smaller range of motion, but because this geometry is not too dependent on the constraints it can be applied to more kinds of origami mechanisms. The first geometry could be used in applications that need less than 15° range of motion, but this is not much for an origami mechanism.

References

[1] Alex Avila et al. “Origami fold states: Concept and design tool”. In: Mechanical Sciences 10.1 (2019), pp. 91–105. ISSN: 2191916X. DOI: 10.5194/ms-10-91-2019.

[2] Zhaowen Lin et al. “Folding at the Microscale: Enabling Multifunctional 3D Origami-Architected Metamaterials”. In: Small 2002229 (2020), pp. 1–9. ISSN: 16136829. DOI: 10.1002/smll.202002229.

[3] Kaori Kuribayashi et al. “Self-deployable origami stent grafts as a biomedical application of Ni-rich TiNi shape memory alloy foil”. In: Materials Science and Engineering A 419.1-2 (2006), pp. 131–137. ISSN: 09215093. DOI: 10.1016/j.msea.2005.12.016.

[4] Agustin Iniguez-Rabago, Yun Li, and Johannes T.B. Overvelde. “Exploring multistability in prismatic metamaterials through local actuation”. In: Nature Communications 10.1 (2019), pp. 1–10. ISSN: 20411723. DOI: 10.1038/s41467-019-13319-7. URL: http://dx.doi.org/10.1038/s41467-019-13319-7.

[5] Cagdas D. Onal, Robert J. Wood, and Daniela Rus. “An origami-inspired approach to worm robots”. In: IEEE/ASME Transactions on Mechatronics 18.2 (2013), pp. 430–438. ISSN: 10834435. DOI: 10.1109/TMECH.2012.2210239.

[6] Magnus H. Kaspersen et al. “Lifting Kirigami Actuators up where they belong: Possibilities for SCI”. In: DIS 2019 - Proceedings of the 2019 ACM Designing Interactive Systems Conference (2019), pp. 935–947. DOI: 10.1145/3322276.3323688.

[7] Tomohiro Tachi, Motoi Masubuchi, and Masaaki Iwamoto. “Rigid Origami Structures with Vacuumatics : Geometric Considerations”. In: Proceedings of the IASS-APCS 2012 (2012), p. 8.

[8] Shuguang Li et al. “A Vacuum-driven Origami “ Magic-ball ” Soft Gripper”. In: (2019), pp. 7401–7408.

[9] Giuseppe Radaelli. “Reverse-twisting of helicoidal shells to obtain neutrally stable linkage mechanisms”. In: International Journal of Mechanical Sciences 202-203.May (2021), p. 106532. ISSN: 00207403. DOI: 10.1016/j.ijmecsci.2021.106532. URL: https://doi.org/10.1016/j.ijmecsci.2021.106532.

[10] Chia Wen Hou and Chao Chieh Lan. “Functional joint mechanisms with constant-torque outputs”. In: Mechanism and Machine Theory 62 (2013), pp. 166–181. ISSN: 0094114X. DOI: 10.1016/j.mechmachtheory.2012.12.002. URL: http://dx.doi.org/10.1016/j.mechmachtheory.2012.12.002.

[11] Ishit Gandhi and Hong Zhou. “Synthesizing constant torque compliant mechanisms using precompressed beams”. In: Journal of Mechanical Design, Transactions of the ASME 141.1 (2019), pp. 1–7. ISSN: 10500472. DOI: 10.1115/1.4041330.

[12] J. G.H. Yee, O. Soykasapt, and S. Pellegrino. “Carbon fibre reinforced plastic tape springs”. In: Collection of Technical Papers - AIAA/ASME/ASCE/AHS/ASC Structures, Structural Dynamics and Materials Conference 5.April (2004), pp. 3305–3313. ISSN: 02734508. DOI: 10.2514/6.2004-1819.

[13] Ömer Soykasap. “Analysis of tape spring hinges”. In: International Journal of Mechanical Sciences 49.7

(2007), pp. 853–860. ISSN: 00207403. DOI: 10.1016/j.ijmecsci.2006.11.013.

[14] T. J.R. Hughes, J. A. Cottrell, and Y. Bazilevs. "Isogeometric analysis: CAD, finite elements, NURBS, exact geometry and mesh refinement". In: Computer Methods in Applied Mechanics and Engineering 194.39-41 (2005), pp. 4135–4195. ISSN: 00457825. DOI: 10.1016/j.cma.2004.10.008.

[15] Heather J. O'Connor, Andrew N. Dickson, and Denis P. Dowling. "Evaluation of the mechanical performance of polymer parts fabricated using a production scale multi jet fusion printing process". In: Additive Manufacturing 22.May (2018), pp. 381–387. ISSN: 22148604. DOI: 10.1016/j.addma.2018.05.035. URL: https://doi.org/10.1016/j.addma.2018.05.035.

[16] Mark Schenk and Simon D. Guest. "Geometry of Miura-folded metamaterials". In: Proceedings of the National Academy of Sciences of the United States of America 110.9 (2013), pp. 3276–3281. ISSN: 00278424. DOI: 10.1073/pnas.1217998110.

4

Discussion

The model and experiment of the proposed negative stiffness crease showed only a short range of motion. This range is not relevant for origami mechanisms. There were also some modeling difficulties encountered. The prestressing of the shell before deforming it meant that the model would often not converge. With a model that can handle these calculations better a search for a longer range of negative stiffness could be done. If this range becomes relevant for origami such a negative stiffness crease could be used for the static balancing of origami mechanisms.

The constant moment crease gave more success. Two geometries were found with a constant moment on a relevant range for origami mechanisms. This constant moment was however dependent on the boundary conditions that were applied to the crease. This was mainly the case for Geometry 3 which could not be optimized into a constant moment crease for boundary conditions other than the initial asymmetric boundary conditions. For Geometry 2 this was however not a problem, with symmetric boundary conditions the crease could also achieve a constant moment.

The results of the prototype experiment were similar to the results of the model. This validates the model. One thing the model does not take into account is hysteresis, this is present in the experiment results. Checking the test setup with a weight attached, instead of the shell, showed little hysteresis. From this, it can be concluded that the hysteresis is inherent to the shell. Manufacturing the shell from a different material, such as a metal could decrease the hysteresis. Getting rid of the hysteresis from the shell is essential for using it in a neutrally stable origami mechanism. For this, two equal constant moment creases are needed, and their constant moments need to be at the same magnitude no matter in which direction they are bending. With hysteresis, the magnitude of the constant moment changes with the bending direction so therefore it is necessary to remove the hysteresis from the shell.

To obtain a moment-angle characteristic with a similar magnitude to the experiment results, the model needed to be adjusted by choosing the right young's modulus. With a Young's modulus of 900 MPa, the experiment results were similar to the model. The Young's modulus of 3D printed PA 12 can be variable and is also dependent on the printing direction. A study by O'Connor [7], showed a Young's modulus around 1200 MPa. This is significantly higher than the Young's modulus used in the model. To verify if the correct Young's modulus is used a three-point bending test could be performed on a flat shell with the same thickness as the prototypes. If the Young's modulus found from this is not similar to the used Young's modulus, but is closer to the 1200 MPa, the magnitudes of the moment-angle characteristics of the prototypes would be smaller than that of the model. This difference in magnitude could be attributed to the variation in the thickness of the shell. It could be the case that the shell is actually thinner than the measured values.

5

Conclusion

In this thesis, an idea is proposed to apply static balancing to origami mechanisms. With an analysis, it is shown that this can be achieved by combining two creases that balance each other. This can be done in two different ways, firstly by combining a negative stiffness crease with a positive stiffness crease, and secondly by combining two constant moment creases.

An initial investigation into a negative stiffness crease was done. Where some insight into the modeling of these types of creases was gained. With the taken approach the negative stiffness range was too short for implementation into origami. However, with a better-suited modeling approach, this range could be increased.

Furthermore, a constant moment crease was designed and tested. This crease showed a constant moment over a range that is suitable to origami mechanisms. The model that was used for the design was also validated with the prototype experiment. Although the constant moment is dependent on what boundary conditions are applied to the crease, with the validated model, creases can be adapted to new boundary conditions.

References

[1] Alex Avila et al. “Origami fold states: Concept and design tool”. In: *Mechanical Sciences* 10.1 (2019), pp. 91–105. ISSN: 2191916X. DOI: 10.5194/ms-10-91-2019.

[2] Mark Schenk and Simon D. Guest. “Geometry of Miura-folded metamaterials”. In: *Proceedings of the National Academy of Sciences of the United States of America* 110.9 (2013), pp. 3276–3281. ISSN: 00278424. DOI: 10.1073/pnas.1217998110.

[3] Zhaowen Lin et al. “Folding at the Microscale: Enabling Multifunctional 3D Origami-Architected Metamaterials”. In: *Small* 2002229 (2020), pp. 1–9. ISSN: 16136829. DOI: 10.1002/smll.202002229.

[4] Binyamin Jasim and Pooya Taheri. “An Origami-Based Portable Solar Panel System”. In: *2018 IEEE 9th Annual Information Technology, Electronics and Mobile Communication Conference, IEMCON 2018* 1 (2019), pp. 199–203. DOI: 10.1109/IEMCON.2018.8614997.

[5] Nima Tolou, Vincent A. Henneken, and Just L. Herder. “Statically balanced compliant micro mechanisms (sb-mems): Concepts and simulation”. In: *Proceedings of the ASME Design Engineering Technical Conference* 2.PARTS A AND B (2010), pp. 447–454. DOI: 10.1115/DETC2010-28406.

[6] Giuseppe Radaelli. “Reverse-twisting of helicoidal shells to obtain neutrally stable linkage mechanisms”. In: *International Journal of Mechanical Sciences* 202-203.May (2021), p. 106532. ISSN: 00207403. DOI: 10.1016/j.ijmecsci.2021.106532. URL: https://doi.org/10.1016/j.ijmecsci.2021.106532.

[7] Heather J. O’Connor, Andrew N. Dickson, and Denis P. Dowling. “Evaluation of the mechanical performance of polymer parts fabricated using a production scale multi jet fusion printing process”. In: *Additive Manufacturing* 22.May (2018), pp. 381–387. ISSN: 22148604. DOI: 10.1016/j.addma.2018.05.035. URL: https://doi.org/10.1016/j.addma.2018.05.035.

[8] Cheng Lv et al. “Origami based mechanical metamaterials”. In: *Scientific Reports* 4.August (2014). ISSN: 20452322. DOI: 10.1038/srep05979.

[9] Hoon Yeub Jeong et al. “3D printing of twisting and rotational bistable structures with tuning elements”. In: *Scientific Reports* 9.1 (2019), pp. 1–10. ISSN: 20452322. DOI: 10.1038/s41598-018-36936-6. URL: http://dx.doi.org/10.1038/s41598-018-36936-6.

[10] T. J.R. Hughes, J. A. Cottrell, and Y. Bazilevs. “Isogeometric analysis: CAD, finite elements, NURBS, exact geometry and mesh refinement”. In: *Computer Methods in Applied Mechanics and Engineering* 194.39-41 (2005), pp. 4135–4195. ISSN: 00457825. DOI: 10.1016/j.cma.2004.10.008.

A

Extra Analysis

For a better understanding of the working of the designed crease, some extra analysis was done. This is briefly explained in the paper, but more detailed in this appendix

A.1. Symmetrical boundary condition

The boundary constraints of the model have a big influence on how the shell behaves. In the paper an asymmetrical boundary condition is used, where one side of the shell is subjected to a moment around the y-axis, and the other side only has a z-direction constraint. This asymmetry was chosen over symmetric constraints because in practice it would be very difficult to perfectly deform a shell symmetrically.

However, an analysis of a shell with symmetrical boundary conditions was still performed. This was done to get more insight into the effects that the boundary conditions have on the moment-angle characteristic of the shell. One side of the shell was fully constrained with an applied rotation around the y-axis, while the other side had an equal but opposite rotation around the y-axis and was constrained in z-direction. This was done for the three optimized geometries that are discussed in the paper, the moment-angle characteristics can be found in Figures A.1-A.3.

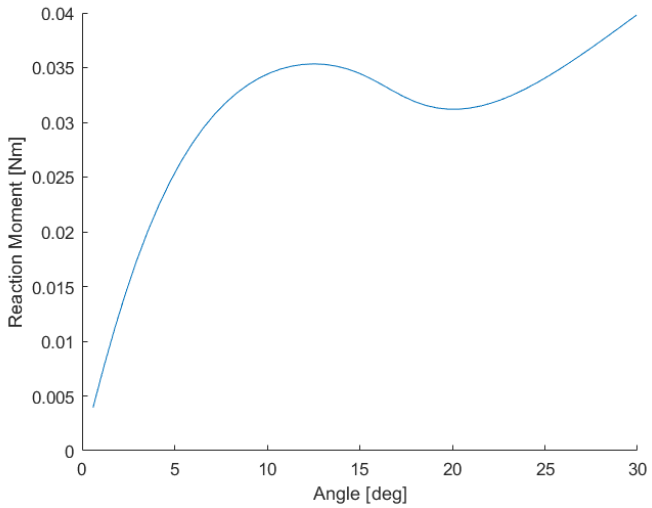

Figure A.1: Moment-angle characteristic of geometry 1 with symmetric constraints, there is no constant moment but it shows potential for an optimization

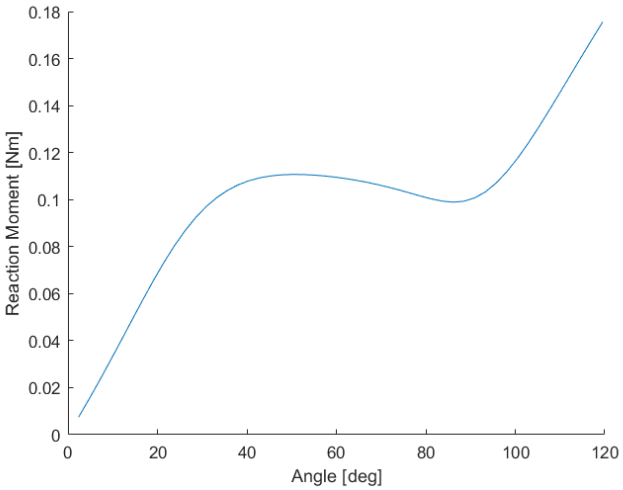

Figure A.2: Moment-angle characteristic of geometry 2 with symmetric constraints, there is no constant moment but it shows potential for an optimization

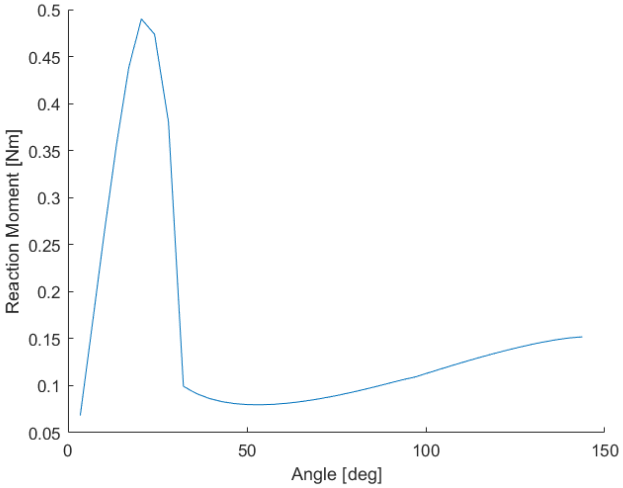

Figure A.3: Moment-angle characteristic of geometry 3 with symmetric constraints, there is no constant moment and not much potential for an optimization

It becomes clear that the boundary constraints have a significant influence on the moment-angle characteristics of the shells. The shells do not show a constant moment anymore. For geometry 1 and 2, the moment-angle characteristics are similar to those that were initially found during the sensitivity study. This shows potential for a new optimization that could deliver a constant moment again. For geometry 3 however, the range where there was previously a constant moment now has a positive stiffness. This proves again that a part of the negative stiffness, that balances the stiffness of the shell, comes from the boundary conditions. Because this negative stiffness part is gone with the new boundary conditions it will be difficult to regain a constant moment with a new optimization, because the negative stiffness needed for that now needs to come from the geometry.

To test this hypothesis the three different geometries were optimized for this new boundary condition with symmetric constraints. The resulting moment-angle characteristics can be seen in Figures A.4 - A.6. For geometry 1 the moment becomes a lot more constant with the optimization, it is only still in a sine shape which the optimizer could not get completely rid of. But with an NRMSE of 0.015, the result is comparable to the optimization for the asymmetric boundary conditions where the NRMSE was 0.013.

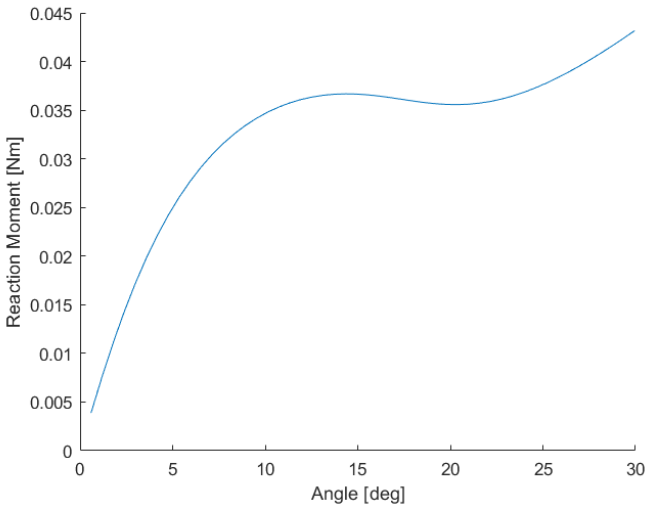

Figure A.4: Moment-angle characteristic of geometry 1 optimized for symmetric constraints, with a constant moment

The optimization of geometry 2 is even better than the optimization for asymmetric boundary conditions. The obtained NRMSE of 0.0004 is 60 times smaller than the NRMSE of 0.024 which was found for the asymmetric boundary conditions. This can be explained by the fact that the shell deforms symmetrically under the symmetric boundary conditions, this means that the part of the shell that provides a constant moment during bending, is now located on both sides of the shell, and both these sides are actuated simultaneously. This doubles the potential range of the constant moment, and keeping the range the same as used with the asymmetrical boundary conditions makes it easier for the optimizer to find a constant moment over this range,

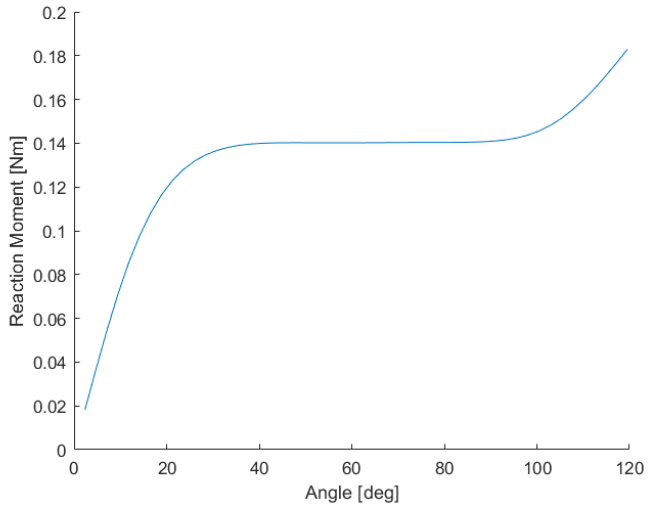

Figure A.5: Moment-angle characteristic of geometry 2 optimized for symmetric constraints, with a constant moment

For geometry 3 no constant moment was found, as expected. Where there was previously a constant moment, there is now a positive stiffness. This means that the negative stiffness that came from the boundary conditions was needed, and could not be replaced by negative stiffness coming from the geometry.

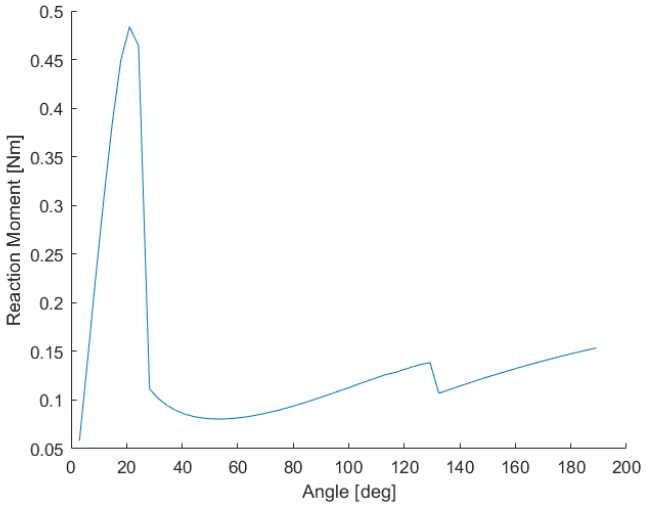

Figure A.6: Moment-angle characteristic of geometry 3 optimized for symmetric constraints, without a constant moment

A.2. Hysteresis in the test setup

The results from the prototype experiment show a lot of hysteresis in the system. To check if this is inherent to the shell, or that it is caused by the test setup an extra experiment was performed. The shell was replaced by a 1 kg mass, which was suspended from the pulley, this can be seen in Figure A.7. The pulley was also connected to the test bench which rotated the pulley, and with that lifted the mass. Then the mass was let down again. The resulting hysteresis loop can be seen in Figure A.8.

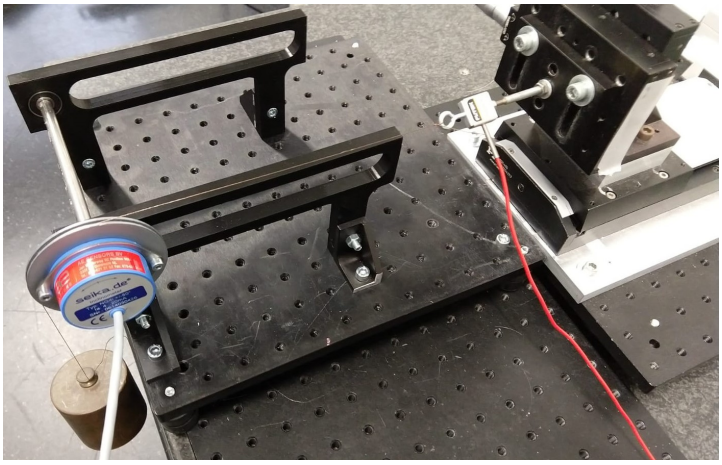

Figure A.7: Test setup with a 1 kg mass instead of a shell

Although a small amount of hysteresis can be seen, this is not nearly as much as observed in the prototype experiments. The average moment while pulling the mass upwards is 0.341 Nm, and the average moment while letting the mass back down is 0.336 Nm. This is 99% of the original moment. From this, it can be concluded that the hysteresis in the prototype experiment is not caused by the test setup.

A.3. Shell measurements

The thickness of the shells that were 3D printed varied between the six shells that were ordered. To know the average thicknesses of the shells they were measured with the use of a micrometer. This on its own was not adequate to measure the thickness of the shell, because a regular micrometer is designed to measure a flat surface between its spindle and anvil. Because the shells are curved the

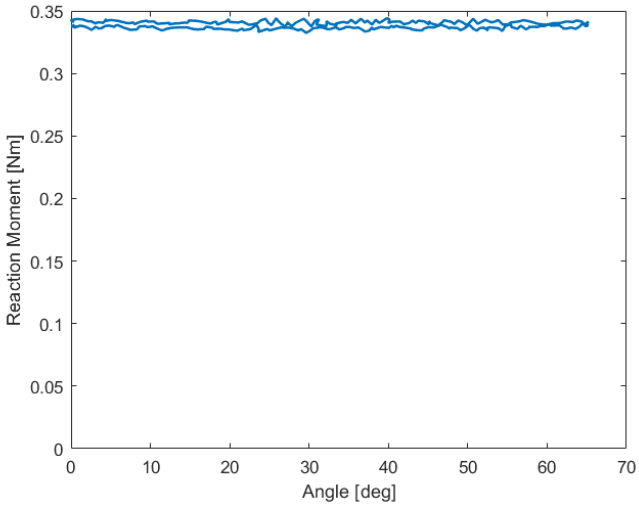

Figure A.8: Hysteresis loop of the test setup with a 1 kg mass, there is only a small amount of hysteresis compared to the prototype experiment

values read on the micrometer will be higher than the real thickness of the shells. This problem can be resolved by measuring the thickness between two point contacts, so two bearing balls were added to the micrometer, this can be seen in Figure A.9.

Each shell is measured on 6 different points which are marked in Figure A.10. The result of the individual measurements, together with the average thickness and the standard deviation can be seen in Table A.1.

Figure A.9: Two bearings are connected to the micrometer to ensure that the thickness of the shell is measured with a point contact

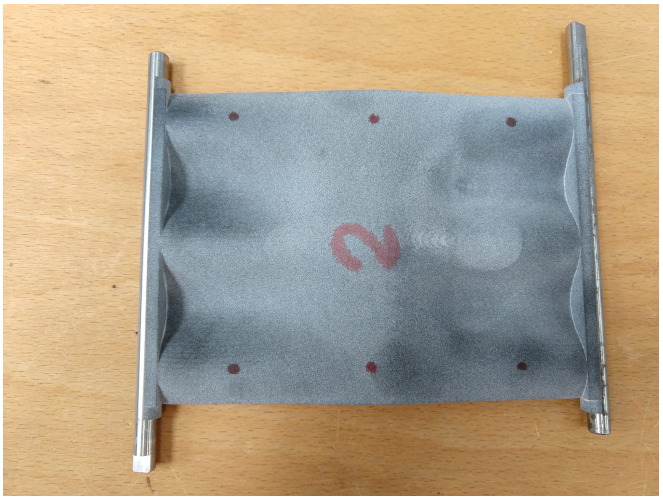

Figure A.10: Shell with markings of where the measurements are done

Measurement:	1 [mm]	2 [mm]	3 [mm]	4 [mm]	5 [mm]	6 [mm]	Avg [mm]	σ [mm]
Prototype 1	0.68	0.68	0.65	0.67	0.68	0.69	0.675	0.014
Prototype 2	0.67	0.65	0.68	0.70	0.61	0.65	0.66	0.031
Prototype 3	0.63	0.66	0.68	0.63	0.59	0.60	0.63	0.034
Prototype 4	0.59	0.61	0.58	0.61	0.55	0.53	0.58	0.033
Prototype 5	0.56	0.56	0.63	0.59	0.53	0.59	0.58	0.034
Prototype 6	0.51	0.48	0.59	0.61	0.56	0.62	0.56	0.056

Table A.1: Measurements of the shells, together with the average and standard deviation

B

Implementation into origami

B.1. Static balancing

A zero stiffness origami mechanism can be achieved with multiple strategies. Two of these are explained in this appendix with the focus on applying it to a Miura-ori tessellation. Firstly, static balancing with a combination of negative stiffness creases and positive stiffness creases is explained. And secondly, static balancing with constant moment creases is explained.

With static balancing two elements are combined in parallel with the goal of making this combination energy neutral. Meaning that the energy level of the combined mechanism does not change while the mechanism is moved. This energy of the system can be plotted in an energy plot, which can be derived by integrating the moment-angle characteristic. So by designing a mechanism with the right moment-angle characteristic, and combining this with another mechanism, an energy-neutral system can be achieved.

B.2. Applied to origami

This combining of mechanisms can be seen in origami as the combining of creases. An origami pattern exists out of multiple facets that are linked together with creases. These creases can be seen as simple mechanisms that bend. For this bending to happen a certain moment is needed. This can be seen in the moment-angle characteristic. However, combining two creases is not that straightforward because a Miura-ori pattern is defined by two different angles. In Figure B.1 these are named α_1 and α_2. These

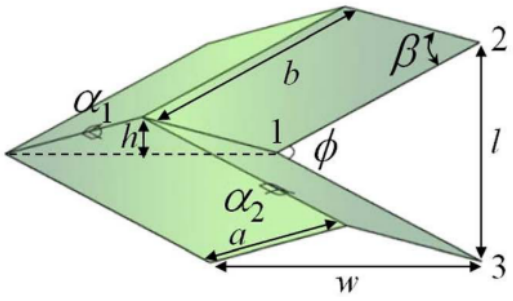

Figure B.1: A unit cell from a Miura-ori tesselation,(Lv [8])

two angles both change differently as the Miura-ori is moved. From Lv [8] we get the formulas of these angles as a function of ϕ:

$$\begin{aligned} \alpha_1 &= \cos^{-1}\left[1 - 2\frac{\sin^2(\phi/2)}{\sin^2\beta}\right] \\ \alpha_2 &= \cos^{-1}\left[1 - 2\cot^2\beta\tan^2(\phi/2)\right] \end{aligned} \tag{B.1}$$

One way of balancing the creases against each other is by balancing one crease that is described by α_1 with another crease that is described by α_2, this will keep the cell symmetrical. For a statically balanced

structure, the sum of the reaction moments of both creases needs to be 0 [Nm] at every angle. So, if the moment-angle diagram of one of the curves is known, this first needs to be translated to the angle of the other crease before they can be balanced out. This translation can be done using the equations from equation B.1. From the first equation ϕ can be written in terms of α_1:

$$\phi = \arccos\left(1 - \sin^2\beta(1 - \cos\alpha_1)\right) \tag{B.2}$$

Then ϕ can be substituted in the equation for α_2, this way α_2 is written as a function of α_1. And the moment-angle characteristics of both creases can be displayed as a function of α_1.

B.3. Negative stiffness

Two elements that can balance each other are a positive and a negative stiffness. A positive stiffness can be found in any normal crease, for a negative stiffness generally a bi-stable mechanism is used. In Figure B.2, the moment-angle characteristics of two hypothetical creases are shown. Crease 1 is bi-stable and has a negative stiffness range, and crease 2 is a normal crease with a positive stiffness that is equal in magnitude to the negative stiffness of crease 1. The combined moment-angle characteristic shows a constant moment, but this is not at 0 [Nm]. Therefore the system is not yet statically balanced.

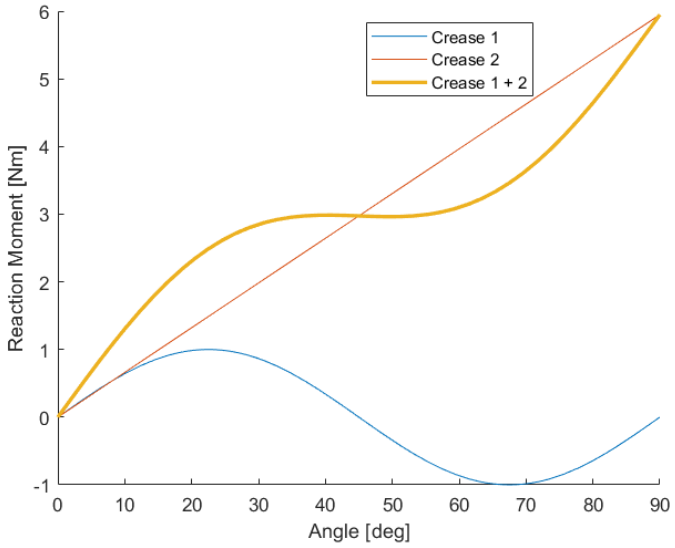

Figure B.2: Moment-angle characteristics of a shell with a partly negative stiffness and a shell with a positive stiffness together with their sum, this combination gives a constant moment at 3 [Nm]

This can still be achieved with these two creases. For this, the moment-angle characteristic of crease 2 needs to be shifted to the right. This shift can be achieved by manufacturing crease 2 into a state where it is in equilibrium at a $45°$ angle. Then when the total system is assembled the crease needs to be bent back to a $0°$ angle. The resulting moment-angle characteristic can be seen in Figure B.3. Now the combined moment-angle characteristic shows a constant moment at 0 [Nm]. In Figure B.4, the energy plots of the creases and the combined system can be seen, and this shows a constant energy for the combined system.

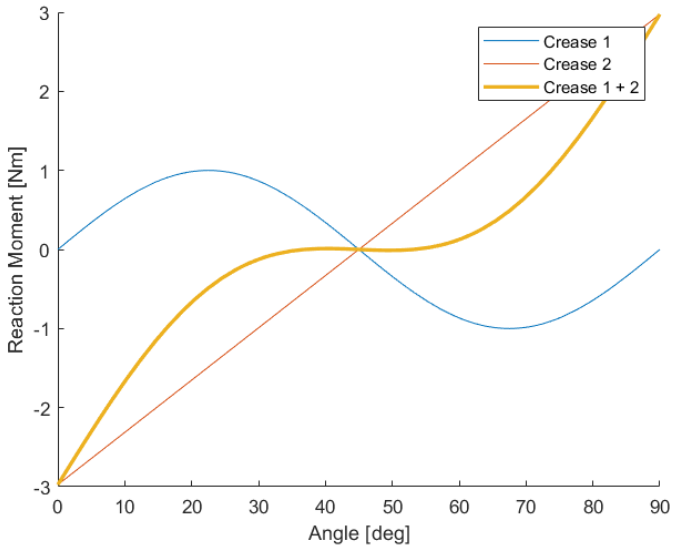

Figure B.3: Moment-angle characteristics of a shell with a partly negative stiffness and a prestressed shell with a positive stiffness together with their sum, this combination gives a constant moment at 0 [Nm]

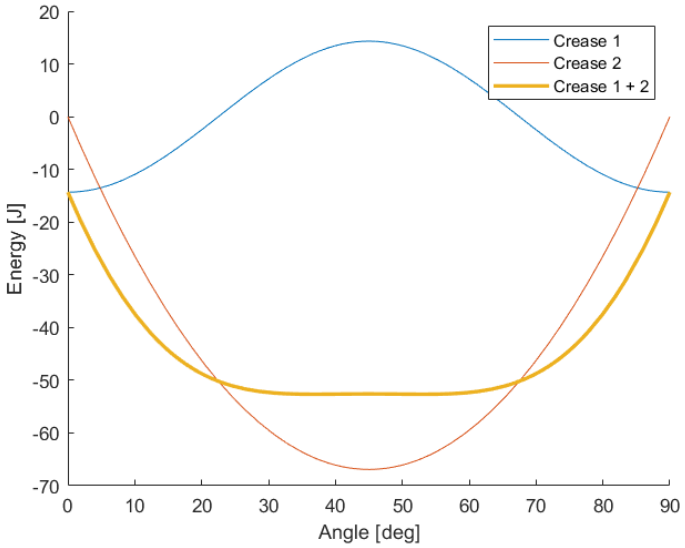

Figure B.4: Energy plot of a shell with a partly negative stiffness and a prestressed shell with a positive stiffness together with their sum, this combination gives a constant energy

B.4. Constant moment

Another way of balancing can be achieved with two constant moments. In Figure B.5, two moment-angle characteristics are shown. These are both of the same hypothetical shell, but because one of these is turned upside down and rotated the other way crease 1 gives a positive constant moment and crease 2 a negative constant moment.

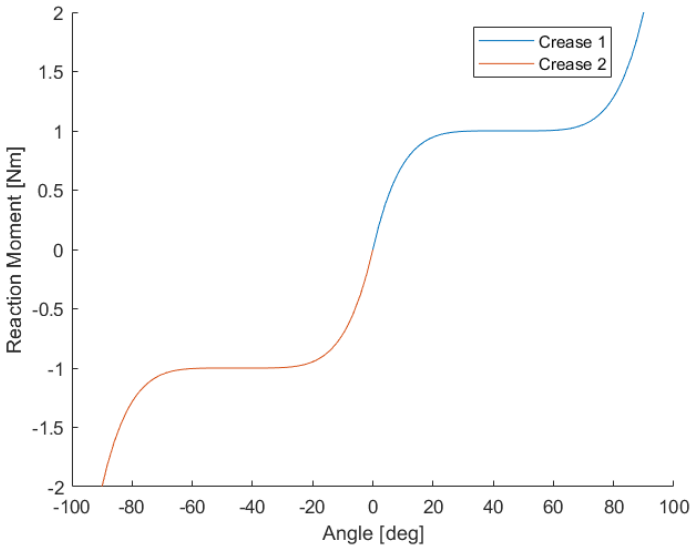

Figure B.5: Moment-angle characteristics of two opposing shells

These two creases in this configuration are not statically balanced, for this their moment-angle characteristics need to be shifted again. In this case, they are shifted 45° towards the middle for both creases. This can be achieved like explained previously by manufacturing the creases under an angle of 45° and bending them back before the assembly. The resulting moment-angle characteristic in Figure B.6 shows a constant moment at 0 [Nm]. And the energy plot in Figure B.7 shows a constant energy.

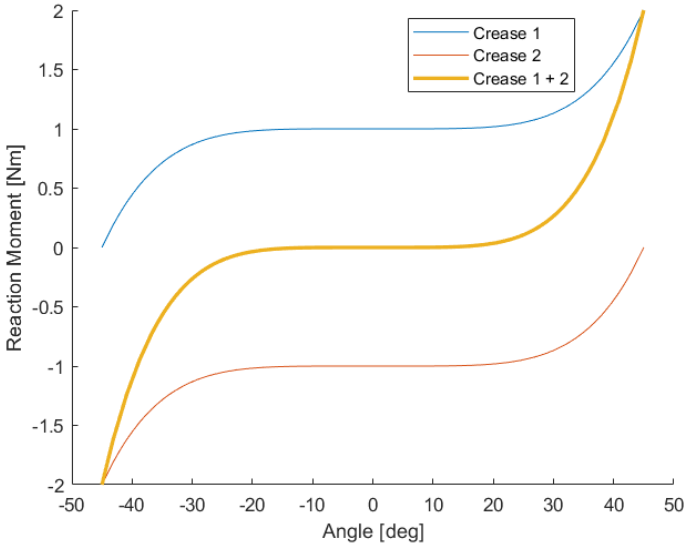

Figure B.6: Moment-angle characteristics of two opposing prestressed shells together with their sum, this combination gives a constant moment at 0 [Nm]

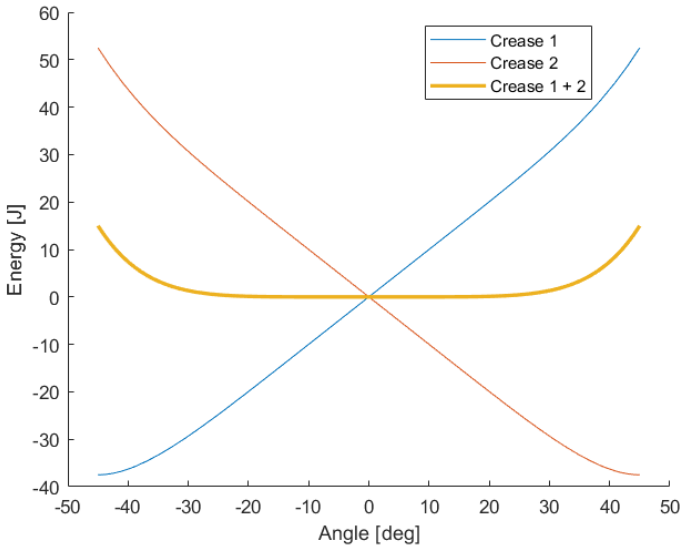

Figure B.7: Energy plot of two opposing prestressed shells together with their sum, this combination gives a constant energy

C

Concept Generation

C.1. Introduction

In this appendix the process of generating the concepts is described. The project was started with the aim to balance an origami mechanism with a combination of a negative stiffness and a positive stiffness crease. So this will be the focus of most of this appendix as well. Later on in the project the focus was shifted to the use of a constant moment crease, this is briefly mentioned in this appendix, but more thoroughly explained in the paper in Chapter 3.

C.2. Concepts

For a zero stiffness origami mechanism, a negative stiffness rotational crease needs to be created. A negative stiffness can often be found in bistable mechanisms, so that is what was looked at. The first concept is a simple strip with a rectangular hole in the middle. The two red points on the sides of this hole are pulled together which gives the strip a saddle shape (Figure C.1b). This results in the strip having two stable states which can be achieved by bending it along its length.

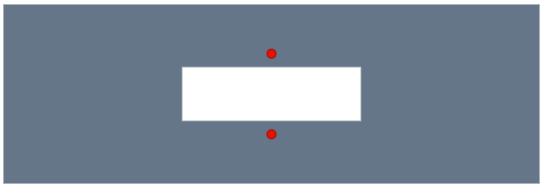

(a) Schematic of concept 1

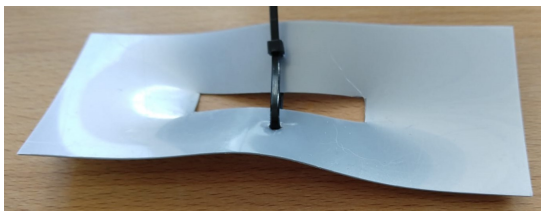

(b) Prototype of concept 1

Figure C.1

The second concept is made from the patterns shown in Figure C.2a. The red lines are connected to each other which causes the middle strip to buckle. This gives the concept its bistability as the middle beam can snap into a convex or concave shape.

(a) Schematic of concept 2

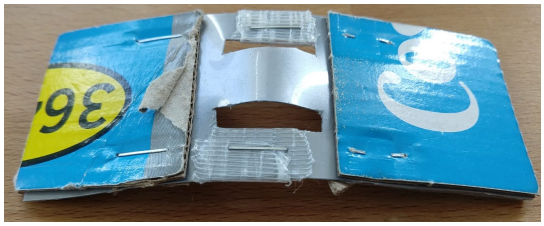

(b) Prototype of concept 2

Figure C.2

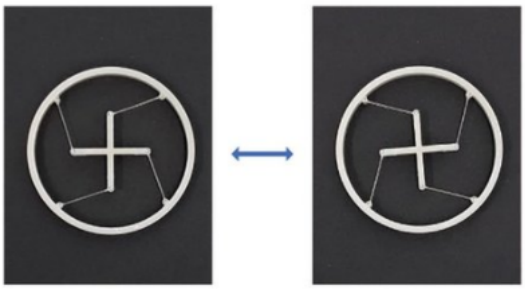

Figure C.3: Concept 3

The third concept comes from Jeong [9], it is a ring with a cross in the middle, the cross is connected to the ring with members that are slightly longer than the minimum distance between the cross and the ring (Figure C.3). As can be seen in the figure this mechanism also has two stable states.

C.3. Evaluation

From the made prototypes the behaviour of the concepts could be evaluated. Concept 1 did have a snap through behaviour which indicates a negative stiffness. However, it did not always bent perfectly along its own length but instead it would twist between the two stable states. This twist felt like the mechanism moved in a shape that had a lower energy level than when it was folded straight. This behaviour was reduced by making more holes in one strip which can be seen in Figure C.4.

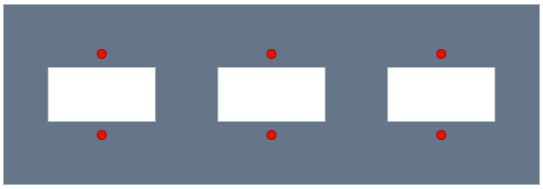

(a) Schematic of concept 1.2

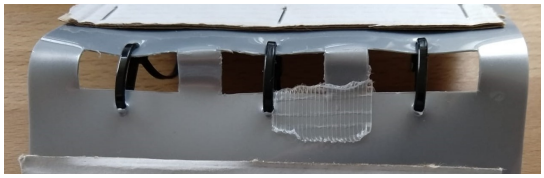

(b) Prototype of concept 1.2

Figure C.4

In the first prototypes the holes are wide, for implementation in an origami mechanism it is preferred to have slimmer creases. This is also possible with this concept which can be seen in Figure C.5. This prototype also showed negative stiffness while being less wide.

Figure C.5: Concept 1.3

The second concept did not show the required behaviour. Although it did have two stable points there was no negative stiffness. To get to the other stable point the mechanism has to be bent past that stable point before the middle strip snaps trough, then the when the mechanism is released it will fold back to its new stable point.

The third concept did work, however it is a complicated design which would be difficult to scale down for applications in origami mechanisms.

Concept 1 is the only concept that shows both a negative stiffness, and a potential to be integrated in an origami mechanism. Therefore, this concept is chosen to be modelled in order to find its exact properties.

C.4. Boundary constraints

The concept of implementation into an origami pattern is based on rigid facets that are connected to the creases. The most straightforward way to connect the crease to the facet is to make a slot where the crease just fits in to, and then clamp the crease into that slot. These clamping beams were 3D printed and had an interface that could easily interact with a test bench. This can be seen in Figure C.6.

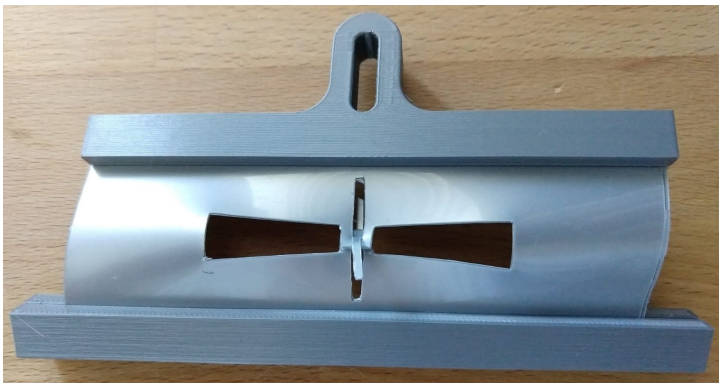

Figure C.6: Fully clamped shell, the shell is slightly twisted

The problem with this method of clamping is that after pre-stressing the two beams are not parallel anymore but they are slightly twisted. This is because due to the pre-stressing the side of the crease is not a straight line anymore but it is curved. Forcing this curve back into a straight slot gives more tension in the shell which deforms it. To solve this problem, the shell was only clamped in on the corners, like in Figure C.7. The holes in the middle of the clamping beam allow the curve in the shell to exist and so there are no extra stresses introduced into the shell.

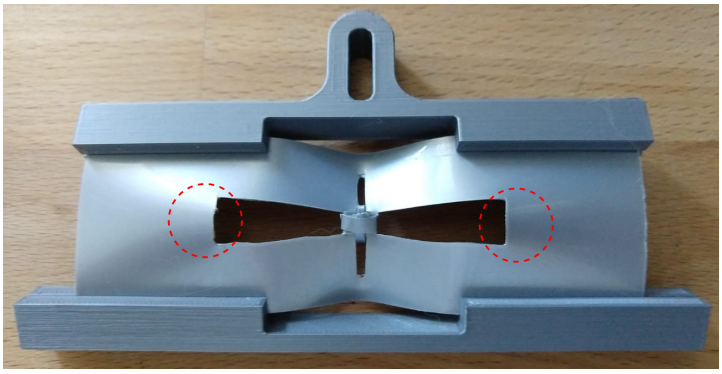

Figure C.7: Shell only clamped on the corners, the shell is not twisted

C.5. Initial testing

On the prototype of this final concept an initial test was done to see how the shell would behave. The lower beam was clamped to the world, while through the loop of the upper beam a rod was placed with two washers connected to either side of the loop. By pulling or pushing on this rod, the washers would move the loop, and with that the shell. The rod was mounted on a testbench, this machine can only move in a straight line, so while the shell was bending the top beam would move in an arc, changing its height. Therefore, the loop is made longer so that it can bend without touching the rod.
The result can be seen in Figure C.8. It can be seen that the negative stiffness region is short, but also that there are two separate regions where there is a negative stiffness. An origami mechanism can only

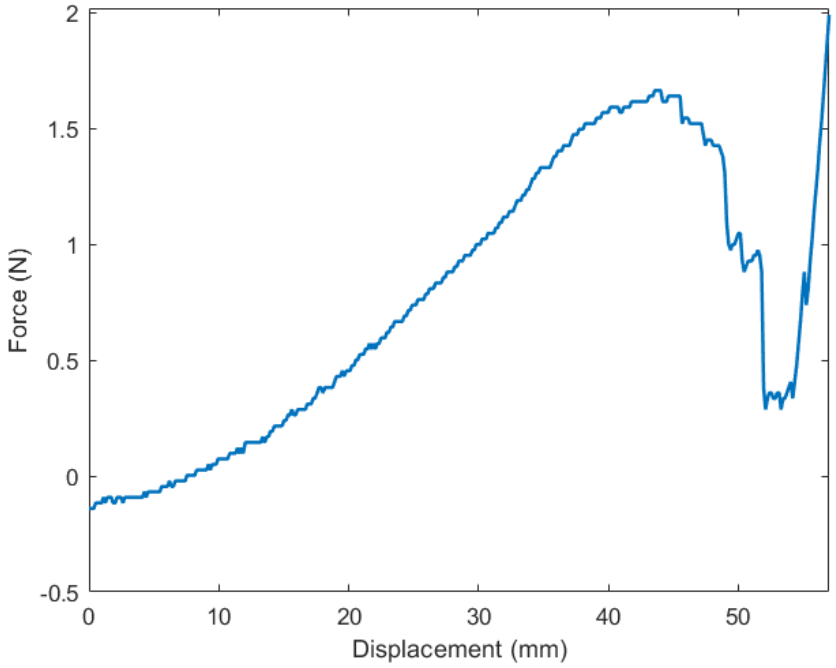

Figure C.8: Force-displacement characteristic of the prototype test, there is only a short range of negative stiffness, as well as a step in the negative stiffness

be balanced over a certain range of motion, and how big this is depends on the length of the negative stiffness. So a short region with negative stiffness can only make an origami mechanisms neutrally stable over a short range of motion. Also the fact that the negative stiffness happens in two stages makes it harder to use for static balancing. When the shell is bend it will eventually snap to its mirrored shape, there are however two points that need to snap to the other side to achieve the mirrored shape, these two points are circled red in Figure C.7. During the testing these two points did not snap through at the same time but one after another, this causes the negative stiffness to be divided into two parts.

C.6. Bowl shape

Fixing the problem of the snap happening at two different times could be done by only using half of the geometry. Then only one snap is needed and there won't be a problem anymore. However, keeping the crease symmetric will probably turn out better when trying to align multiple creases. So another solution would be to move the gaps to the outside, and keep the ridge that buckles in the middle. This way the two points that need to snap through are connected and might influence each other. Prototypes of this concept can be seen in Figure C.9. Here the first prototype has a long ridge between the two holes. So here the two points circled in red are far apart which still allows them to snap one by one. In the second prototype the ridge is shorter and these two points are closer together. Because of this, the two points in this prototype both snap at the same time.

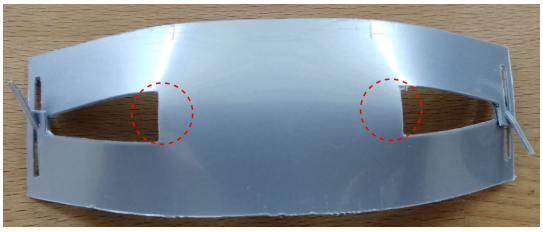

(a) Bowl shaped shell with more space between the gaps, the red circles highlight the points that need to snap through

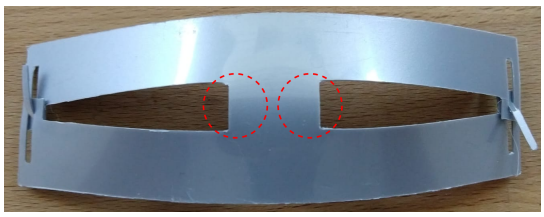

(b) Bowl shaped shell with less space between the gaps, the red circles highlight the points that need to snap through

Figure C.9

C.7. Convex crease with corrugated facets

With the current concept there are a few obstacles that are difficult to overcome. The negative stiffness that is achieved so far does not show much potential for the use in an origami mechanism due to its small range of motion. Also the facets that the creases are supposed to be combined with turned out too big and heavy for the creases. On the modeling side the combination of the rigid clamping, and needed pre-stress makes it hard to create a realistic model. More on this can be found in Appendix D.

To create a mechanism that can be modelled realistically a few thing need to change. The clamping had a big influence on the deformation of the shell, this is because it was very close to the crease, which deforms. If the clamping can be placed further away from the crease, it should have less of an effect on the deformation of the crease. By adding the facets already in the model this can be achieved. This means that the facets need to be the same thickness as the creases. The facets are kept stiffer than the creases by using a corrugation in the facets. This way the geometry provides most of the stiffness. Because prestressing also brought problems for a realistic model, the new crease should not depend on prestressing for its negative stiffness. For this the bowl shape was chosen. In a prestressed state the bowl already showed negative stiffness and a bistable behaviour. This combined resulted in a convex shaped crease, with two corrugated facets on the sides, this can be seen in Figure C.10.

Figure C.10: Concept with a convex crease and corrugated facets

Because the new concept does not use prestress it is likely that the crease will not be bistable. Even with the convex shape, the initial position of the crease will have a energy level of zero, an inverted position will have a higher energy level, and is possibly not even stable. This has consequences for finding negative stiffness in the crease. What is more likely is that what would have been a negative stiffness for a prestressed crease will now transform into a zero stiffness due to the stiffness of the shell which will be added to it. However, this should not be a problem as with a zero stiffness, or constant moment, a neutrally stable origami pattern can still be achieved. This is explained in Appendix B.

D

Modeling

D.1. Crumple zone

The previously explained concept is modeled in the ShellMech software, this is an isogeometric analysis framework [10], which is based on the Kirchhoff-Love plate theorem and a linear isotropic material law. A geometry can be created by defining control points in a 3D space, a surface is made up of B-splines that are attracted to these control points. This surface is then given a thickness which results in a shell. This shell can be deformed and the stresses and reaction forces can be calculated from this. One limiting factor is that the software can only work with continuous shells, this is a problem for our concept as there is a hole in it. To overcome this, the hole is replaced by a so-called crumple zone (Figure D.1). This allows the shell to more easily deform in the middle as if there was a gap in the geometry.

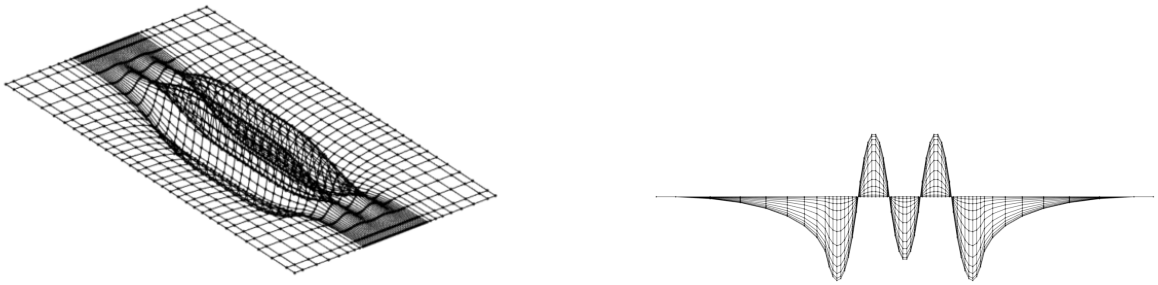

(a) Geometry of the model with a crumple zone

(b) Side view of the model with a crumple zone

Figure D.1

The prestress is modeled by applying two equal and opposite forces on the red points from Figure C.1b. These forces deform the shell to its prestressed state in the first iteration of the solver. The distance between the two points where the force is applied is locked after which a second solution is made where the shell is bent along its length with this it is possible to evaluate the moment-angle diagram of the shell and to see if there is negative stiffness.

The geometry is defined by a grid of control points through which a spline is drawn. The control points that correspond to the geometry of Figure D.1 can be seen in Figure D.2. This grid is defined by 7 variables which are defined in Figure D.3, here the front and side views of the grid are shown together with the variables.

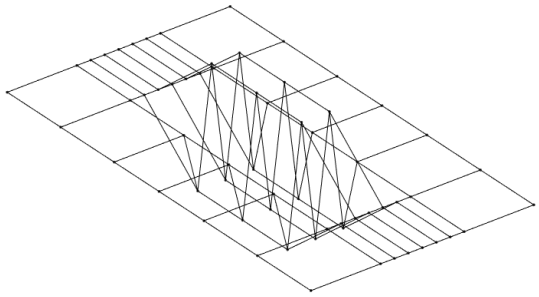

Figure D.2: Grid of control points of the geometry

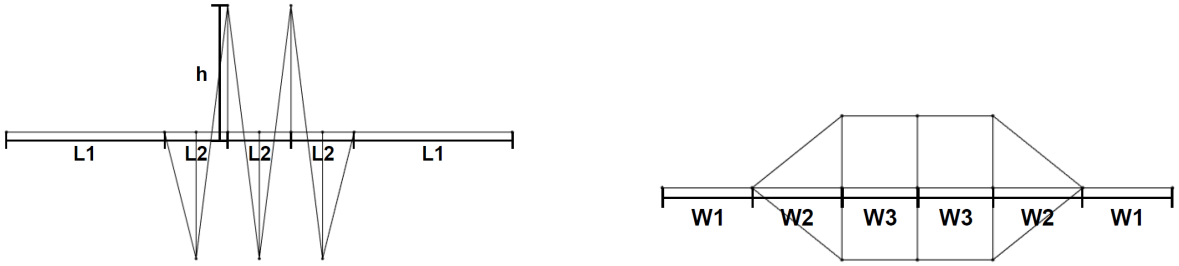

(a) Front view of the grid, with the used variables

(b) Side view of the grid, with the used variables

Figure D.3

To get a better picture of these shells' possible moment angle characteristics, the variables were individually varied. For each variable, except for L2, 5 different values were used, and for all these slightly different shapes the moment angle diagrams were obtained. This whole process was done for 4 different variations on the geometry where the number of ridges in the crumple zone was changed. The example in Figure D.1 has 5 ridges, the other models had 1, 3, and 7 ridges. The resulting moment angle diagrams can be found in figures D.4 through D.7. The titles of the smaller graphs indicate which variable is varied, and the red dots indicate the local minima and maxima. This is done to get a better view of the length of the negative stiffness regime.

What becomes apparent from these figures is that for all the combinations that were used the range of negative stiffness never exceeded more than $5°$. This is unfortunately too small to be relevant for origami mechanisms. An attempt was made to optimize the geometry for a longer range of negative stiffness. For this, the local maximum and minimum were found, the objective was the angle at the local maximum minus the angle at the local minimum. However, this did not yield much better results. This was in part because the local minimum and maximum are discrete, they are dependent on the time steps that the model takes. So if one of these extremes suddenly shifts a time step a very different result was found. This could be improved by increasing the number of time steps, however, this would also increase the calculation time. This was also part of the problem, the model already took a long time to calculate the deformations of the complex shape. These two problems combined made it very difficult to optimize the geometry.

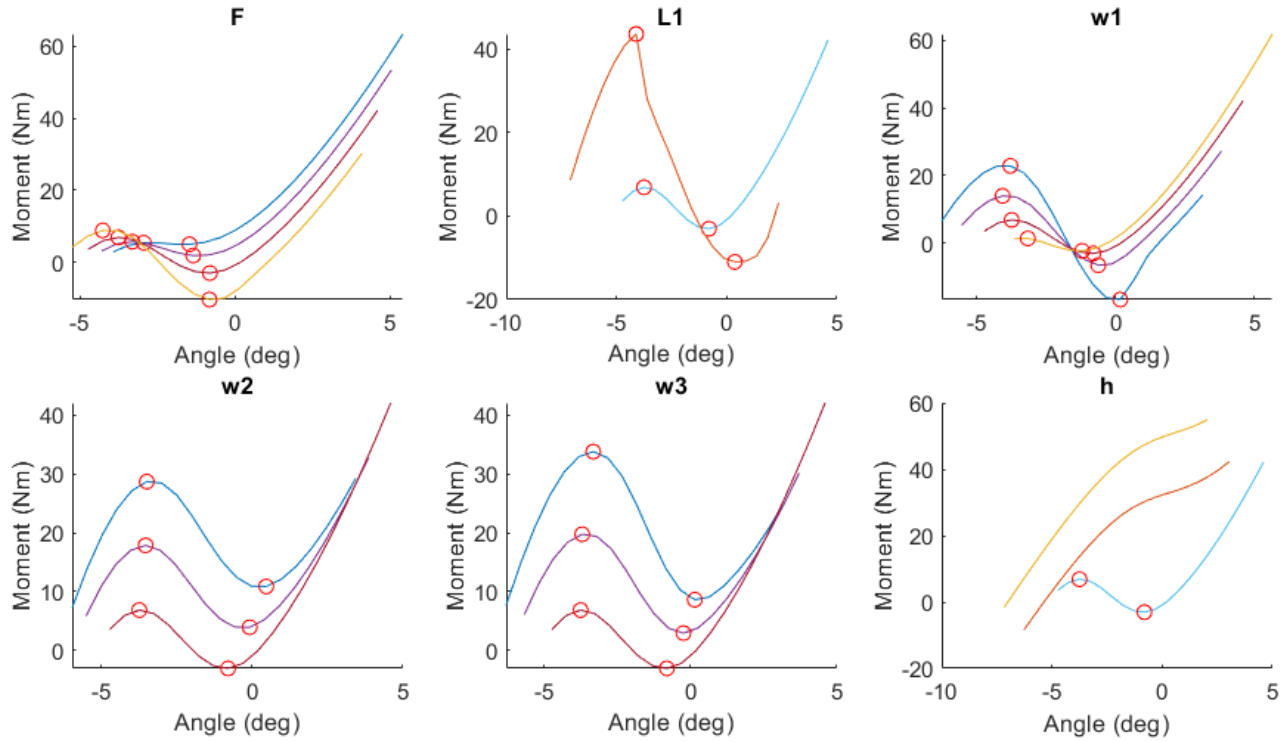

Figure D.4: Moment angle diagrams of the shape with one ridge

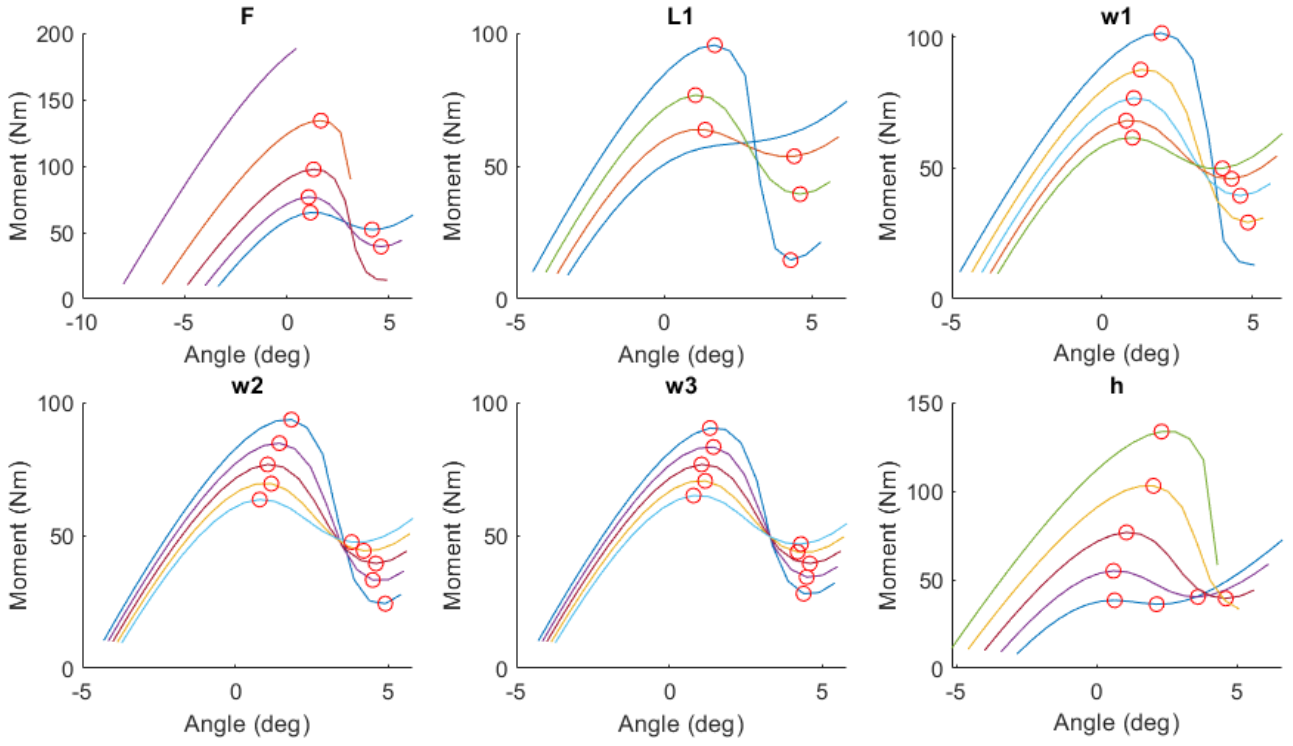

Figure D.5: Moment angle diagrams of the shape with three ridges

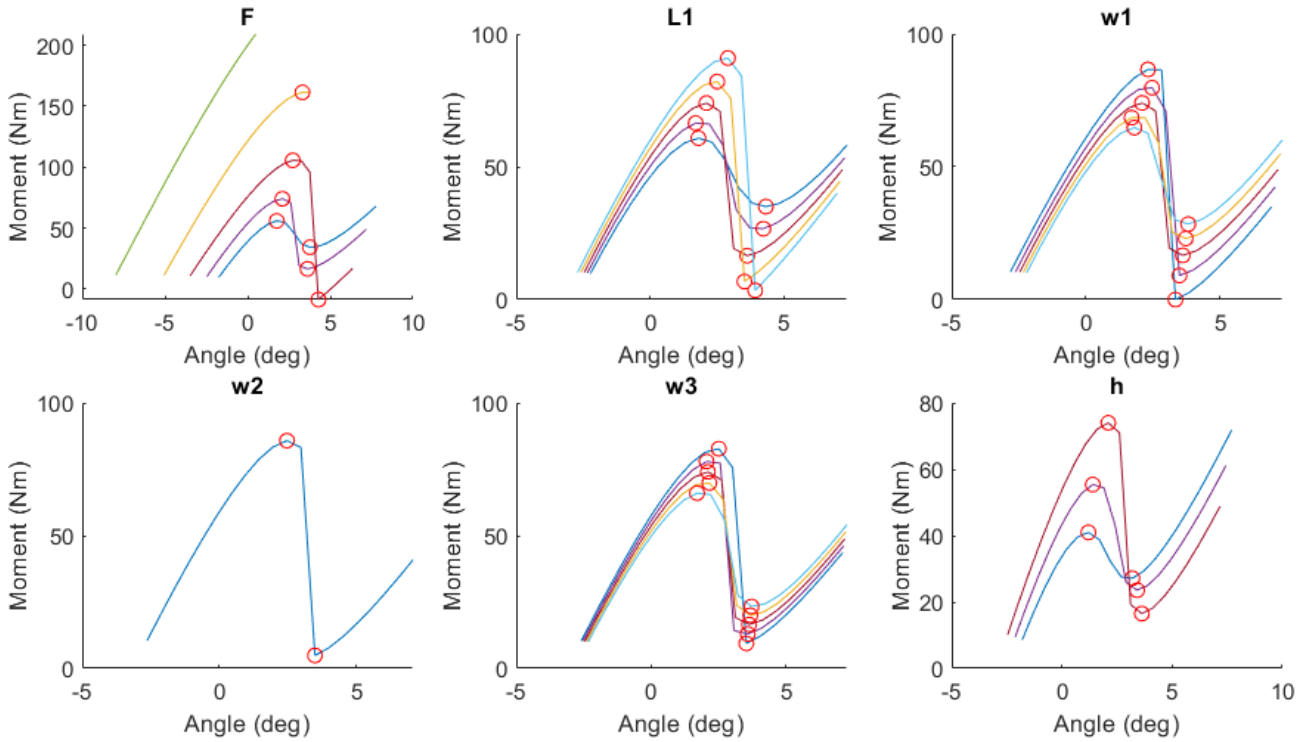

Figure D.6: Moment angle diagrams of the shape with five ridges

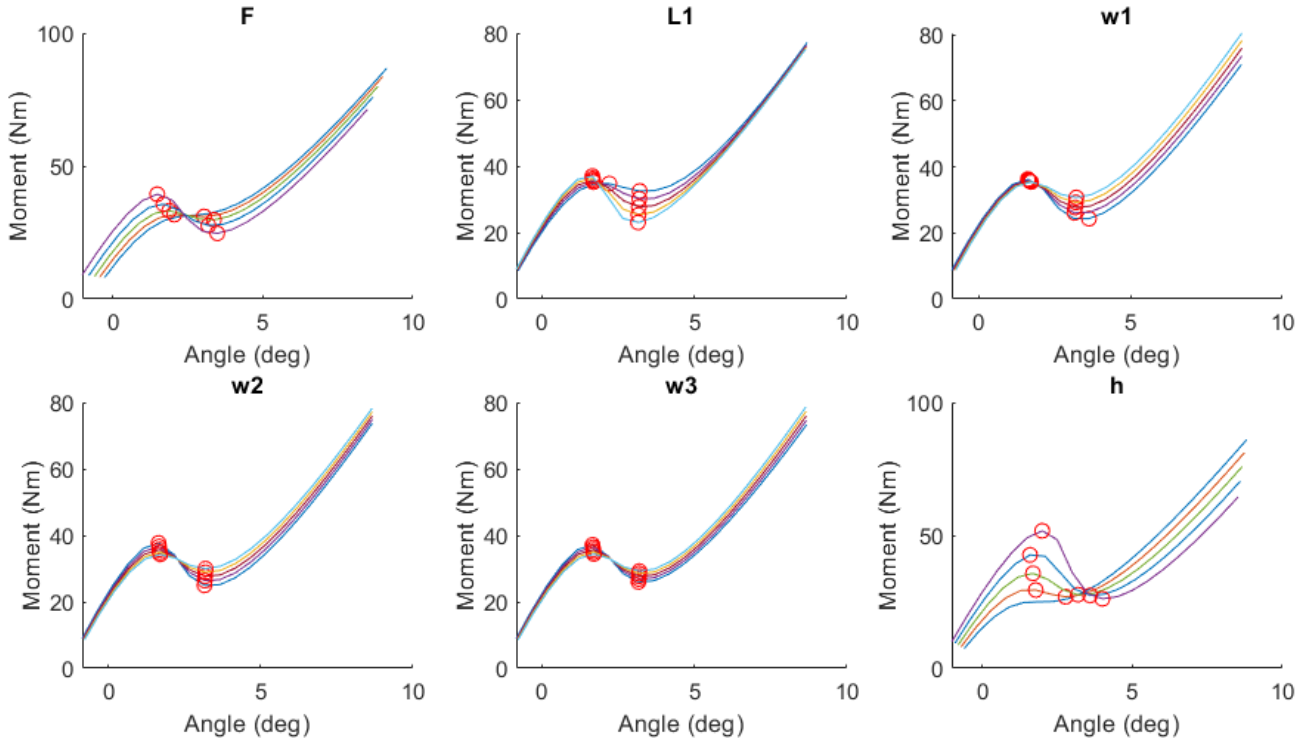

Figure D.7: Moment angle diagrams of the shape with seven ridges

D.2. Hole with decreased thickness

As was just explained, a drawback of this crumple zone is that the more ridges are implemented the more complex the geometry becomes. There are more points needed on the grid to define the geometry, this causes longer computation times for the code, which came especially apparent during the optimization process. Therefore, a simpler solution was implemented, by staying more true to the original concept of a shell with a hole in it. Because the code still can only work with continuous shells a true hole can't be modeled. But the thickness of the shell can be decreased at the place where the hole should be (Fig. D.8).

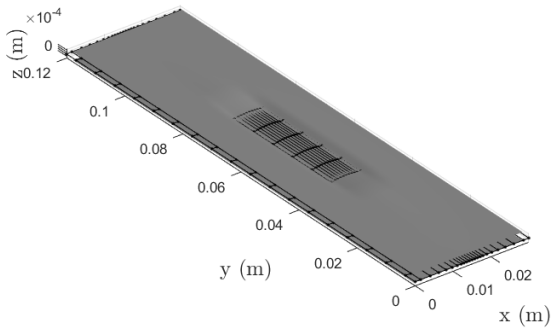

Figure D.8: Model with decreased thickness

Another improvement that was made is the way of prestressing. The forces pulling the hole together were replaced by bending the shell. The distance between the two points is still locked after the shell is bent. The shell is then bent back the other way to analyze its moment-angle characteristic. Prestressing the shell with the use of bending is more constant. The exact angle that the shell should bend to can be used as an input. When using the two forces for the prestressing the prestress angle is not only dependent on these forces, but also on how easily the geometry deforms. So the prestress angle between two different shells can vary for the same prestress force. Another problem with using the force for prestressing is the lack of a moment arm in the new geometry. This new geometry is flat, and adding a force will not bend the shell. For this to happen a small extra force perpendicular to the shell is needed, to give it an initial bending.

Just like the model of the crumple zone the sides of the crease are modeled as fully clamped. From prototyping, it became apparent that this did not work well, and only clamping the corners showed better results. To simulate this in the model, the beams in the middle could not just be deleted. That would mean that the middle beam nodes were floating free and the solver would be unable to solve this. So instead, the stiffness of the middle beams was decreased to simulate a lack of clamping. There are two ways to define the beams, firstly, beam nodes are connected one after another, and the corner nodes also connect to the pilot point. The second method is to connect each node separately to the pilot point. This second method is a lot stiffer. The stiffness of the clamp can be decreased by combining these two methods. This is done by connecting the outer nodes directly to the pilot point, and the middle node to each other as per the first method to define the beams. This can be seen in Figure D.9, where the beams are shown in blue.

There was still a difference between the modeling and the prototype. Namely, the shell in the model is completely clamped in all directions. In the prototype however the shell is clamped into a slot which still allows it to contract along this slot, which in the model is along the y-axis. At this point, however, the model depended on too many approximations, such as the hole, which is just a patch with a decreased thickness, and the clamping of the middle that is still there, only less stiff than the clamping on the outside. Therefore a new concept was used.

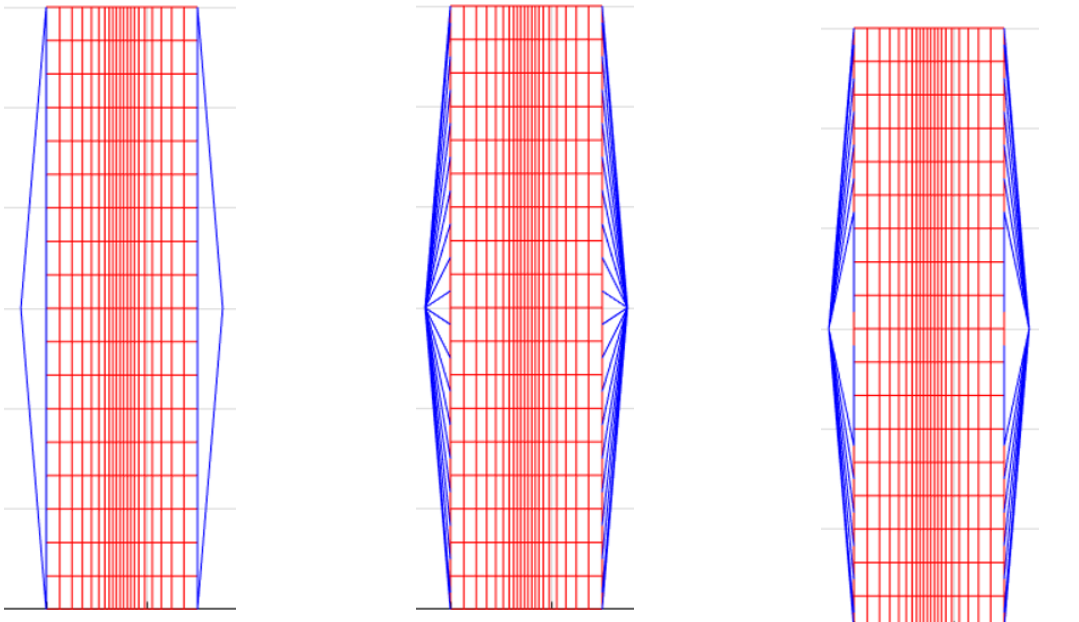

(a) First method with directly connected beam nodes

(b) Second method with beam nodes connected to pilot point

(c) Combination of the two methods

Figure D.9

D.3. Convex crease

The new concept can be found in Appendix C. For this concept first a sensitivity study was performed, and later the concept was optimized.

D.3.1. Sensitivity analyses

The problems that there were so far with the model can be solved with a new concept where a convex crease is used in combination with corrugated facets. The rigid beams are connected to these corrugated facets, and because the facets are already stiffer than the crease they should not deform much. This means that the rigid beams do not have much influence on the deformation of the shell. The new concept can also be modeled as a continuous shell, which the used FEM program was designed for. Finally, the shell does not need to be prestressed anymore, which means less calculation time.

The control points of the facets are defined by the parameters from Table D.1 and Figure D.10. The corrugations are equally spaced along the length of the shell. And the end of the taper connects to the side of the crease. The control points of the crease are arranged in a 3x7 grid, and all lie on an ellipsoid. This ellipsoid is located between the two facets and is defined by a rectangle made up of the crease width and the length, the ellipsoid height, and a scaling factor in y-direction. The ellipsoid is drawn through the four corners of the rectangle, with the ellipsoid height being the distance in z-direction between the corners of the rectangle and the highest point on the ellipsoid. Finally, a scaling factor is used to define the circularity of the ellipsoid. This scaling factor scales the radius of the ellipsoid in y-direction compared to the radii in x- and z-direction.

W_f	Flange width
W_t	Taper width
W	Crease width
L	Length
H_c	Corrugation height
H_e	Ellipsoid height
S_y	Scaling factor of ellipsoid in y-direction

Table D.1: Parameter definitions

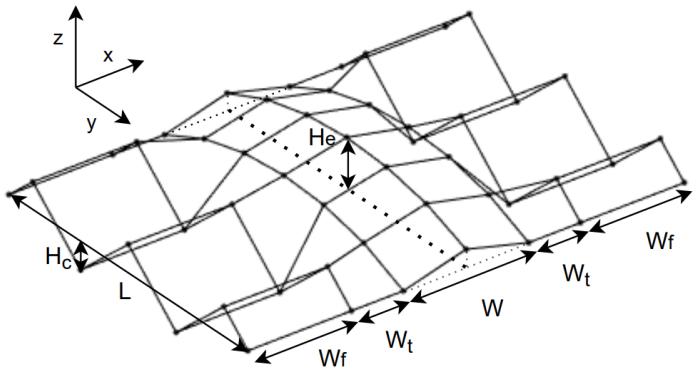

Figure D.10: Parameters that define the geometry

D.3.2. Optimization

An optimization of the shell was done to find the geometry with the best moment-angle characteristic. The objective that needs to be minimized is the flatness between two points. The flatness of the interval is defined as the normalized Root Mean Square Error (RMSE) with respect to the average moment on that interval. First, this average moment is calculated using equation D.1. Here n is the number of data points on the interval. With this average, the RMSE and normalized RMSE are calculated according to equations D.2 and D.3.

$$\hat{M} = \frac{\sum_{i=1}^{n} M_i}{n} \tag{D.1}$$

$$\text{RMSE} = \sqrt{\sum_{i=1}^{n} \frac{\left(\hat{M} - M_i\right)^2}{n}} \tag{D.2}$$

$$\text{Normalized RMSE} = \frac{\text{RMSE}}{\hat{M}} \tag{D.3}$$

If the moment is constant over the whole interval a new optimization is done over a longer interval, with the result of the previous optimization as a starting point. This is repeated until there is no longer a constant moment over the interval.

This was firstly performed with the fminsearch algorithm from the MATLAB optimization toolbox, and the optimization parameters W, H_e, and S_y.

For a better optimization of the shell, more freedom was given to the geometry, which allowed the optimizer to find a better result. The control points of the crease are no longer defined by an ellipsoid. They still consist out of a 3 by 7 grid, however, the heights of the seven points through the middle are defined by 4 independent parameters, namely H1, H2, H3, and H4. The height of the points on the side is dependent on the height of their adjacent point, and scaled by a scale factor S. This is visualized in Figure D.11. In this second optimization, the used optimization parameters were H1, H2, H3, and H4.

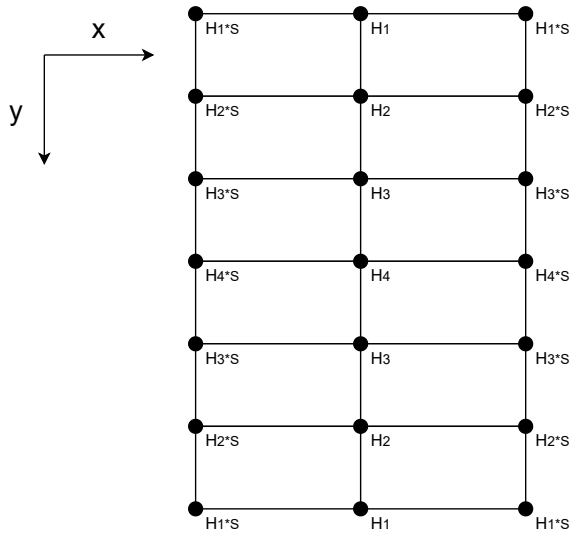

Figure D.11: 2D representation of new optimization parameters